

(NASA-CR-197624) CROSS-TAIL
CURRENT, FIELD-ALIGNED CURRENT, AND
B(y) (New Hampshire Univ.) 60 p

N95-19032

Unclas

G3/46 0038395

Cross-Tail Current, Field-Aligned Current, and B_y

38395

RICHARD L. KAUFMANN, CHEN LU, AND DOUGLAS J. LARSON

p. 60

Department of Physics, University of New Hampshire, Durham, NH 03824

Abstract. Orbits of individual charged particles were traced in a one-dimensional magnetic field model that included a uniform cross-tail component B_{y0} . The effects of B_{y0} on the cross-tail current distribution $j_y(z)$, the average cross-tail drift velocity $\langle v_y(z) \rangle$, and the average pitch angle change $\langle \Delta\alpha \rangle$ experienced during current sheet encounters were calculated. The addition of a B_{y0} that exceeded several tenths of one nanotesla completely eliminated all resonance effects for odd- N orbits. An odd- N resonance involves ions that enter and exit the current sheet on the same side. Pitch angles of nearly all such ions changed substantially during a typical current sheet interaction, and there was no region of large cross-tail drift velocity in the presence of a modest B_{y0} . The addition of a very large B_{y0} guide field in the direction that enhances the natural drift produces a large j_y and small $\langle \Delta\alpha \rangle$ for ions with all energies. The addition of a modest B_{y0} had less effect near even- N resonances. In this case, ions in a small energy range were found to undergo so little change in pitch angle that particles which originated in the ionosphere would pass through the current sheet and return to the conjugate ionosphere. Finally, the cross-tail drift of ions from regions dominated by stochastic orbits to regions dominated by either resonant or guiding center orbits was considered. The ion drift speed changed substantially during such transitions. The accompanying electrons obey the guiding center equations, so electron drift is more uniform. Any difference between gradients in the fluxes associated with electron and ion drifts requires the presence of a Birkeland current in order to maintain charge neutrality. This plasma sheet region therefore serves as a current generator. The analysis predicts that the resulting Birkeland current connects to the lowest altitude equatorial regions in which ions drift to or from a point at which stochastic orbits predominate. The proposed mechanism appears only in analyses that include non-guiding-center effects.

1. ORBIT TYPES AND MAGNETOTAIL REGIONS

A number of studies have traced charged particle orbits in taillike magnetic field models. *Chen* [1992] reviewed this topic with particular emphasis on the dynamics of particle orbits. The one-dimensional modified *Harris* [1962] model

$$\begin{aligned} B_x(z) &= B_{x0} \tanh(z/L) \\ B_y(z) &= 0 \\ B_z(z) &= B_{z0} \end{aligned} \quad (1)$$

has been employed in many of these analyses. The constant parameters B_{x0} , B_{z0} , and L can be selected so that, within the current sheet, the shapes of Harris-type field lines are similar to the shapes of magnetotail field lines in the more comprehensive *Tsyganenko* [1989] or T89 model [*Kaufmann et al.*, 1993a, hereafter referred to as paper 1]. Since one-dimensional models cannot have a point at which $B_z = 0$, they are not able to represent the midtail plasma sheet boundary layer (PSBL) or lobes. In this work, we investigate particle motion only within the inner portion of the central plasma sheet (CPS). Equation (1) was used at $|z| < L$ and

$$B_x(z) = \frac{B_{x0}}{\eta} \tanh[(z/L)^\eta] + B_{x0} \left[1 - \frac{1}{\eta} \right] \tanh(1) \quad (2)$$

with $\eta = 5$ was used when $|z| > L$. Equation (2) was selected because it provides a smooth cutoff in the cross-tail electric current density, $j_y(z) = dB_x/dz$, between $|z| = L$ and $|z| = 4L/3$. Beyond this point, which generally is well within the plasma sheet, particles carry little cross-tail current and orbit tracing can be stopped.

Invariant Tori

A charged particle moves along the surface of a torus in phase space, or of a torus in ordinary x, y, z coordinates for the one-dimensional magnetic field considered here [*Büchner and Zelenyi*, 1989]. The entire torus is ring-like for a class of ions that remain trapped within the principal current sheet (Figure 1a). These ions continually bounce or meander back and forth across $z = 0$.

When projected onto the y - z plane, the ring-like or crossing trajectories resemble a figure 8. This orbital shape is especially important in studies of $j_y(z)$. Ring-like or figure 8 ions carry current in the positive y direction at the largest $|z|$ they reach, and in the negative y direction near $z = 0$.

For some orbits the earthward part of a torus (right side of Figures 1b and 1c) splits into two segments, one in the northern and one in the southern hemisphere. The curve on which the torus splits is called an orbital separatrix. An ion bounces back and forth across $z = 0$ while on the ring-like segment (left sides of Figures 1b and 1c) and spirals around a magnetic field line while on the split segments of a torus. This ion crosses one separatrix when it enters the ring-like segment and one when it leaves. Depending on its pitch angle, the ion either may mirror during the spiraling portion of the orbit, or it may escape in a one-dimensional model. Mirroring trajectories also are referred to as cucumber orbits. Such ions are trapped in the sense that they remain within the CPS, but differ from the figure 8 or ring-type trapped orbits because mirroring ions do not remain within the principal current sheet.

Orbital Parameters

The magnetic moment, $\mu = mv_{\perp}^2 / (2B)$ is commonly used as an approximate invariant of the motion when nonrelativistic ions spiral around magnetic field lines. Such particles are characterized by $\Omega \gg \omega_b$, where Ω is the local gyrofrequency and ω_b is the bounce frequency between mirror points. The guiding center approximations are nearly obeyed at large $|z|$ on the split or spiral segments of a torus, so that μ is nearly conserved on this non-crossing portion of an orbit.

The action integral $I_z = (2\pi)^{-1} \oint p_z dz$ [Speiser, 1970; Sonnerup, 1971] is approximately conserved while particles bounce back and forth across $z = 0$ on the ring-like or crossing portion of an orbit. This part of an orbit is characterized by $\omega_z < \Omega_{z0}$, where ω_z is the north-south bounce frequency across the $z = 0$ plane and $\Omega_{z0} = qB_{z0}/m$ is the gyrofrequency based on B_{z0} . In general, neither I_z nor μ is conserved during separatrix crossings.

Büchner and Zelenyi [1986; 1989] introduced the κ parameter

$$\kappa = B_{z0} \left[\frac{Lq}{B_{x0} m v} \right]^{1/2} \quad (3)$$

which, together with I_z or μ , helps to organize the dominant trajectories found in a given region of the tail. In the model field used here, $\kappa^2 = R_c / \rho_{z0}$ where R_c is the magnetic field line radius of curvature at $z = 0$ and $\rho_{z0} = v / \Omega_{z0}$. Thermal ions and electrons have $\kappa > 2$ in the radiation belts and near-Earth tail. These particles spiral around magnetic field lines and obey the guiding center equations during all or almost all of an orbit. There is at most a very short ring-like region near $z = 0$ where the northern and southern segments join. Particles with $\kappa > 2$ only cross the $z = 0$ plane once during each current sheet interaction, and they drift from dawn to dusk during this brief period.

Guiding center motion breaks down for most ions beyond a point that usually is located somewhere between $5 R_E$ and $15 R_E$ in the magnetotail [Pulkkinen *et al.*, 1992; paper 1]. We refer to that portion of the non-guiding-center region in which $2 > \kappa > \kappa_r \equiv B_{z0} / B_{x0}$ as the midtail. It is convenient to divide the associated ions into categories according to κ . Groups of ions with different κ carry substantially different cross-tail current distributions $j_y(z)$, and suffer different average pitch angle changes $\langle \Delta\alpha \rangle$ during a current sheet interaction. The primary goal of this work is to study $j_y(\kappa, z)$ and $\langle \Delta\alpha(\kappa) \rangle$. These two parameters were selected because they can be evaluated using satellite data, and because of their importance in determining the structure of the plasma sheet.

Stochastic and Resonant Orbits

Both μ and I_z of nearly all ions with certain values of κ (e.g., $\kappa = 0.82, 0.40$, and 0.27) are substantially different before and after almost every current sheet interaction. These orbits are called stochastic or chaotic. Most stochastic ions eventually leave the current sheet with such a small pitch angle that they escape from a one-dimensional model field. The adiabatic invariants μ and I_z change primarily during the pair of separatrix crossings that occur as particles move from a split

torus to a ring-like orbit segment and then back.

A second class of ions which follow split tori in the midtail are called resonant. The magnetic moment and I_z of these ions also change substantially during most orbital separatrix crossings. However, at certain resonant values of κ (e.g., $\kappa = 0.53$, 0.32 , and 0.23) the changes in μ and I_z at a pair of crossings nearly cancel for a wide range of incident pitch and phase angles [Büchner, 1991]. Resonant ions tend to follow very simple, predictable orbits. For example, nearly all $\kappa = 0.53$ ions cross the $z = 0$ plane just twice during each interaction with the current sheet. These ions appear to simply bounce off the current sheet. Figure 1b was generated by following a single $\kappa = 0.53$ ion while it mirrored and returned several times to the outer CPS. It was necessary to use a resonant ion to illustrate this structure so that nearly the same torus was followed after each encounter with the current sheet. The $\kappa = 0.53$ ion in Figure 1b was injected at $z > 0$, so it always entered and left the current sheet on the northern side. Figure 1b therefore illustrates only half of a full split torus. An ion injected at $z < 0$ would follow a similar trajectory that entered and left the southern side of the current sheet. Figure 1c was prepared by simply adding a reflected duplicate of the trajectory in Figure 1b. Figure 1c therefore illustrates a full split torus. Figures 1b and 1c are shown from different viewpoints to more clearly illustrate all aspects of the torus.

Ions injected at the northern edge of the CPS at the next resonance ($\kappa = 0.32$) pass through $z = 0$ three times and then move into the southern outer CPS. Such ions would alternately follow the northern and southern segments of a torus similar to that in Figure 1c. However, whenever the changes in μ and I_z at a pair of separatrix crossings do not exactly cancel, the ion will mirror at different locations and therefore be on a different torus during successive orbits. We found it is difficult to identify $\kappa = 0.32$ ions for which cancellation was exact enough over a wide enough range of pitch and phase angles so that a single torus would be followed throughout several orbits.

At the N th resonance the angle variable θ_z associated with the action I_z changes by $\Delta\theta_z = N\pi$ [Büchner and Zelenyi, 1989; 1990]. With this definition of N , the $\kappa > 2$ guiding center motion cor-

responds to $N = 0$, and $\kappa = 0.53$ resonant ions have $N = 1$. The relationship between N and κ is approximately

$$N = \frac{0.80}{\kappa} - 0.5 \quad (4)$$

[Chen, 1992; Ashour-Abdalla et al., 1993; Kaufmann and Lu, 1993c, hereafter referred to as paper 2].

Nonresonant Orbits

The κ of a typical thermal ion decreases as one moves farther out the magnetotail. The average ion velocity decreases slowly with increasing distance [Baumjohann et al., 1989]. In the T89 Kp = 4 model, L increases slowly and B_{x0} decreases rapidly as one moves out the tail (paper 1). For example, L changes approximately 30% while B_{x0} changes by a factor of 2 between $x = -10$ and $-20 R_E$. The point $\kappa = \kappa_r$ is reached when $\rho_{x0} = L$ or $LqB_{x0} / (mv) = 1$, where ρ_{x0} is the ion gyroradius in a magnetic field B_{x0} . An ion with $\kappa > \kappa_r$ does not have enough energy to go directly from $z = 0$ to $|z| = L$ without being either reflected back toward $z = 0$ or being deflected onto a spiral orbit. Note that the condition $\kappa = \kappa_r$ depends upon L , v , and B_{x0} but not on B_{z0} since it is B_x that causes the reflection of an ion. The ring-like segment of an invariant torus, and therefore the separatrix, are confined to $|z| < L$ for ions with $\kappa > \kappa_r$.

When $\kappa < \kappa_r$, orbits following split tori become insensitive to κ so that stochastic and resonant effects are not obvious. We refer to these as nonresonant orbits. Burkhardt and Chen [1991] showed that resonant peaks in the average stochastic trapping time disappear abruptly at $\kappa = \kappa_r$. Nonresonant ions experience relatively little change in α during a current sheet encounter (paper 1). On the ring-like segment of a split torus, a nonresonant ion with appropriate pitch and phase angles can bounce back and forth between north-south reflection points that are well beyond $|z| = L$. If many such ions were present, they would carry substantial j_y well beyond the edge of the current sheet. Therefore, only a small number of ions can exist with these pitch and phase angles in

any self-consistent current sheet, in which the particles must carry the correct $j_y(z)$ distribution to generate the magnetic field in which their orbits were traced.

In papers 1 and 2 we studied the pitch angle changes and current carrying properties of various groups of resonant ions in the $B_{y0} = 0$ modified Harris field. The present paper is primarily a study of the effect of nonzero B_{y0} on $j_y(z)$ and $\langle \Delta\alpha \rangle$. It is found that changes in B_{y0} can produce some of the same macroscopic effects that previously were associated with changes in κ when $B_{y0} = 0$. However, we find that the odd- and even- N orbits behave quite differently. The most striking effect is that odd- N resonances vanish when B_{y0} exceeds several tenths of one nanotesla.

Finally, the field-aligned currents which are expected if κ or B_{y0} varies along a drift path are discussed. This rather speculative field-aligned-current generation mechanism is included because of its potential importance to magnetosphere-ionosphere coupling.

2. CROSS-TAIL MAGNETIC FIELDS

Overview with $B_{y0} = 0$

Figure 2 shows how $j_y(z)$, the distribution of cross-tail current carried by a group of monoenergetic ions, depends on κ when $B_{y0} = 0$. Groups of ions with randomly selected pitch and phase angles were injected at $z_i = L$ into a model magnetic field ($B_{x0} = 32$ nT, $B_{y0} = 0$, $B_{z0} = 3.3$ nT, $L = 1 R_E$). As is common in one-dimensional studies, this analysis was carried out in a reference frame with $E_y = 0$. Pitch angles were selected to have the same distribution as would be found in a bi-Maxwellian plasma with $T_{\parallel}/T_{\perp} = 10$, while phase angles were selected from an isotropic distribution. The structure in Figure 2 also can be seen when $T_{\parallel}/T_{\perp} = 1$, but is more clearly defined with the larger ratio. We are interested in distributions with large T_{\parallel}/T_{\perp} at $|z| = L$ partly because they are required to produce force balance in a self-consistent one-dimensional model (paper 2). Another reason for injecting groups with large T_{\parallel}/T_{\perp} is to study particles that reach low- and middle-altitude satellites. All ions in any one group were injected with the same energy rather

than with energies selected from a Maxwellian distribution so they would all have the same κ .

The region $|z| < 4L/3$ was divided into 40 boxes, each having a width $\Delta z = L/15$. Since our model is symmetric, results at positive and negative z were added to yield plasma parameters in each of 20 boxes between $|z| = 0$ and $4L/3$. The density $n(z)$ and electric current distribution $j_y(z)$ were evaluated for each group by keeping track of the time spent and the distance each ion moved across the tail while it was in a given box (paper 2). Since the absolute value of $j_y(z)$ depends on particle energy, B_{x0} , and B_{z0} , we plot a normalized average cross-tail ion velocity instead of $j_y(z)$. The average velocity $\langle v_y(z) \rangle$ is given by $j_y(z) / [qn(z)]$, where q is the ion charge. The vertical axis in Figure 2 is $\langle v_y \rangle / v_o$, where v_o is the total ion velocity. This normalized cross-tail velocity peaks at more than 0.5 near $z = 0$ at each of the first three resonances. The peaks extend to larger $|z|$ as κ gets smaller. Figure 2 also shows that $\langle v_y \rangle / v_o$ is small at all z for stochastic ions, such as those with $\kappa = 0.40$ or 0.82 .

Simple models of B_y

Satellites frequently observe magnetotail fields with large components in the geocentric solar magnetospheric y direction. However, not all such observations can be modeled by a modified Harris field (1) that includes a constant nonzero B_{y0} . The sketches in Figure 3 illustrate several reasons why satellites observe a substantial B_y . The remaining sections of this paper describe effects of only one of these sources.

A dipolar field has a large B_y everywhere except near noon and midnight. The apparent dragging of magnetospheric field lines into the tail by a force in the equatorial plane (Figure 3a) reduces B_y in the midtail. However the distorted field lines in a tail of varying width retain a positive B_y at $y < 0$ and a negative B_y at $y > 0$ in the northern hemisphere, as shown. The direction of this B_y is reversed in the southern hemisphere and is zero at the neutral sheet. The magnetic field distortion shown in Figure 3a is primarily produced by currents inside the Earth and by the magnetopause and cross-tail current systems. Field-aligned sheet currents also contribute to the distur-

tions sketched in Figure 3a. If the region 1 current system flows in the outer CPS or PSBL in the midtail, then field lines in the inner CPS will have a larger $|B_y|$ than do field lines in the lobes.

Figure 3b shows another reason why satellites observe magnetic fields in the solar magnetospheric y direction. The neutral sheet is shown tipped, with \mathbf{B} everywhere perpendicular to the sheet. Dipole tilt is known to produce substantial warping of the neutral sheet [Fairfield, 1979; Tsyganenko, 1989]. Since $B_x = 0$ at $z = 0$ in (1), this equation can describe the fields in Figure 3b in a tipped neutral sheet coordinate system, with z measured normal to the neutral sheet. The particle orbits in this tipped coordinate system are correctly described using (1) with $B_{y0} = 0$. Warping is generated by the same current systems that were discussed above.

Figure 3c shows the only type of B_y that will be investigated here. In this case, \mathbf{B} is no longer normal to the neutral sheet. A uniform B_{y0} is added throughout the entire current sheet to describe this field. The two ends of a field line in Figure 3c reach Earth at different longitudes. When $B_{y0} > 0$, the northern ionospheric footpoint of a magnetotail field line is duskward of the southern footpoint. A B_y that is uniform throughout the tail is generated by currents outside the magnetosphere. We place our model current sheets at infinity. This type of magnetotail B_y usually is described in terms of penetration or leakage of the y component of the interplanetary magnetic field (IMF) into the magnetosphere. As noted above, region 1 Birkeland sheet currents can produce a relatively uniform B_y in the inner CPS, and a different relatively uniform B_y in the lobes.

Observed B_y

There have been a number of studies of B_y in the midmagnetotail. Measurements also have been made at synchronous orbit [Cowley and Hughes, 1983] and in the distant tail [Sibeck et al., 1985]. We are most interested in the midtail within $60 R_E$ of Earth, where the T89 magnetosphere model can be used to estimate the parameters in (1). Fairfield [1979] removed the average effects of tail flaring, aberration due to motion of the Earth around the sun, and neutral sheet warping to determine the residual B_y . A correlation with the measured IMF B_y yielded an average 13% pene-

tration for the IMP 6 data set, taken throughout the plasma sheet and lobes between $x = -20$ and $-33 R_E$. *Lui* [1984] used an IMP 6 data set that was restricted to neutral sheet crossings. He obtained an average 50% penetration of the IMF B_y . *Sergeev* [1987] used ISEE 1 data between $x = -15$ and $-23 R_E$. He separated plasma sheet and lobe data, finding an average 60% penetration in the plasma sheet and 15% in the lobes. This difference in B_y between the two regions was attributed to the effect of region 1 sheet currents in the PSBL.

Kaymaz et al. [1994] carried out an extensive study of B_y using IMP 8 magnetotail data taken between $x = -25$ and $-40 R_E$. They found an average 26% penetration when $|z| < 8 R_E$ and 9% when $|z| > 8 R_E$. These z values were corrected for average warping effects. However, this study showed that the penetration of B_y is more complex than can be modeled by a constant B_{y0} . The measured B_y was much stronger in the flanks than near midnight. This observation suggests that IMF B_y penetration may be closely associated with processes that take place within or near the LLBL.

A uniform positive B_{y0} could be modeled by a uniform current sheet flowing earthward at large positive z , either outside the northern magnetopause or in the northern mantle, and a similar tailward flowing current sheet in the southern hemisphere. One way to model the observed enhanced B_y in the flanks would be to have the current sheets at large $|z|$ become stronger as $|y|$ increases. Another possible model would have a uniform current sheet in the mantle and also reversed currents near midnight in the PSBL (tailward in the north and earthward in the south when B_y is positive). We previously evaluated $j_{||}$ for the T89 Kp = 5 model [*Kaufmann et al.*, 1993b]. This model has no average uniform B_y because it was based on a large data set taken both when the IMF B_y was positive and negative. However, it may be significant that the T89 model showed the largest magnitudes of $j_{||}$ at large $|z|$ in the flanks.

Kaymaz et al. [1994] also found an average neutral sheet tilt (Figure 3b) that correlated with IMF B_y . The average tilt angle was 7° . The neutral sheet was tilted in a direction which increases

the need for a nonzero model B_{y0} in (1). For example, when B_y was negative, as shown in Figure 3b, the neutral sheet was found to tip in the direction opposite from that shown in our sketch. This same distortion had been found in the distant tail by *Sibeck et al.* [1985]. However, once again the *Kaymaz et al.* [1994] study shows the magnetotail is substantially more complex than our model. They found the tilt angle much larger than the 7° average in the flanks and much smaller than the average, or even reversed, near midnight.

The above observations suggest that some B_y usually should be added to (1) in the midtail current sheet. The uniform B_{y0} we use may be appropriate when following a single orbit, in which an ion moves only $1 R_E$ in the y direction. However, a substantially more complex B_y field will be needed in a three-dimensional study. The average IMF $|B_y|$ is approximately 2 nT, so it appears that the average uniform part of $|B_y|$ is on the order of 1 nT in the neutral sheet, and several tenths of one nanotesla at larger $|z|$. Larger fields are required in the flanks, and the observed fluctuations suggest that several nanotesla B_y fields can be found almost anywhere at times. The following sections show how a uniform B_{y0} with such magnitudes affects particle dynamics and the structure of the current sheet.

3. ENERGIZATION

Constants of the Motion

In the original *Harris* [1962] magnetic field model ($B_{y0} = B_{z0} = 0$), the Hamiltonian $H(\mathbf{P}, \mathbf{r}) = c \{ [\mathbf{P} - q\mathbf{A}(\mathbf{r})]^2 + m^2 c^2 \}^{1/2}$ and both the x and y components of the canonical momentum [$P_x = \gamma m v_x$, $P_y = \gamma m v_y + qA_y$, where $\gamma = (1 - v^2/c^2)^{-1/2}$] are constants of the motion. The Harris vector potential usually is written with only a y component

$$A_y = -B_{x0} L \ln [\cosh (z/L)] \equiv A_H \quad (5)$$

The Poisson brackets $[H, P_x]$, $[H, P_y]$, and $[P_x, P_y]$ all are zero, so that the three constants of the motion are independent, or are in involution.

The addition of a nonzero B_{z0} to an infinite one-dimensional current sheet, as in (1) and (2),

can be described by modifying A_x , A_y , or both. The dynamics of orbits in this modified Harris model were studied by *Chen and Palmadesso* [1986] and by *Büchner and Zelenyi* [1989]. When $\mathbf{A}(\mathbf{x})$ is evaluated using

$$\mathbf{A}(\mathbf{x}) = \int d\mathbf{x}' \left[\frac{\mathbf{j}(\mathbf{x}')}{|\mathbf{x} - \mathbf{x}'|} \right] \quad (6)$$

then selecting $A_x = 0$, $A_y = B_{z0}x + A_H$ corresponds physically to generating the uniform B_{z0} by adding infinite current sheets located at $x = \pm\infty$, with current flowing in the $\pm y$ directions. In this case, only H and P_y are independent constants of the motion. Use of this gauge is reasonable if B_{z0} is produced primarily by distant cross-tail currents. Another simple gauge, in which $A'_x = -B_{z0}y$ and $A'_y = A_H$, yields H and $P'_x = \gamma m v_x + qA'_x$ as constants of the motion. Physically, this suggests producing B_{z0} by adding sheet currents at $y = \pm\infty$ with current flowing in the $\mp x$ directions. This gauge therefore is appropriate if B_{z0} is produced primarily by currents flowing in the flanks. Since both forms of \mathbf{A} yield identical magnetic fields, either can be used to follow particle motion. However, *Chen and Palmadesso* [1986] showed that even though P_y and P'_x are both constants of the motion, they are not independent. Their Poisson bracket is nonzero, $[P'_x, P_y] = \gamma m \Omega_{z0}$. A consequence of not having three independent constants of the motion is the possible appearance of stochastic particle orbits.

Here we repeat the analysis of *Chen and Palmadesso* [1986] using $B_y(z) = B_{y0}$. The new vector potential can be written in simple gauges by adding either $B_{y0}z$ to A_x or by adding $-B_{y0}x$ to A_z . The former corresponds physically to the creation of B_{y0} in the one-dimensional model by adding two current sheets located at $z = \pm\infty$ with current flowing in the $\pm x$ direction. This gauge suggests B_{y0} is created by field-aligned currents in the mantle, or in the PSBL when only the inner CPS is modeled. The latter gauge corresponds to introducing sheets at $x = \pm\infty$ with current flowing in the $\mp z$ direction. Since there are two simple ways to introduce B_{z0} by modifying the original Harris \mathbf{A} and two equivalent ways to introduce B_{y0} , \mathbf{A} can be written in any of these 4

simple gauges. Two forms have $A_y = B_{z0}x + A_H$, both of which yield $P_y = \gamma m v_y + qA_y$ as a constant of the motion. The third form has $A'_x = B_{y0}z - B_{z0}y$ so that $P'_x = \gamma m v_x + qA'_x$ is a constant of the motion. The fourth form of \mathbf{A} yields no constant component of \mathbf{P} . Since all 4 forms of \mathbf{A} yield identical \mathbf{B} fields, there are again a total of 3 constants: H , P_y and P'_x . Even though the above expressions for P_y and P'_x are different in the model with $B_{y0} = 0$ than in the model with $B_{y0} \neq 0$, the Poisson bracket $[P'_x, P_y] = \gamma m \Omega_{z0}$ is the same. This suggests that stochastic particle motion is possible in both cases. We will see below that the most striking consequence of adding a modest B_{y0} is a substantial change in the simple resonant behavior described in Section 1.

E Fields and Acceleration

For one-dimensional models with a uniform $B_z(z) = B_{z0}$, a uniform $E_y(z) = E_{y0}$ in the Earth reference frame is transformed so that $E'_y = 0$ as seen in a frame moving Earthward at $u_x = E_{y0}/B_{z0}$, the deHoffman Teller frame. Our and many other analyses were done in this moving (primed) frame. When $B_{y0} = 0$, all other components of \mathbf{E} or \mathbf{B} as measured in the Earth frame are equal (to order $\gamma - 1$) to the components measured in the moving frame.

When $B_{y0} \neq 0$, both E_y and E_z differ significantly in the two reference frames. The moving frame was selected so that $E'_y = 0$. Because guiding-center electrons and non-guiding-center ions are not distributed in the same manner along a field line, it was not possible to maintain charge neutrality throughout the current sheet unless a sheath-like electric field E'_z was included [Eastwood, 1974; paper 2]. With 3-keV protons and 3/8-keV electrons, the potential difference between $z = 0$ and $z = L$ was found to be approximately 200 V in the moving frame for most cases studied. The resulting E'_z ranges from approximately 0.03 mV/m for a quiet time current sheet with $L = 1 R_E$ to approximately 0.6 mV/m for an extremely thin current sheet with $L = 0.05 R_E$. In comparison, the steady E_{y0} in the Earth frame is approximately 0.15 - 0.3 mV/m if there is a uniform 50 - 100 kV potential drop across a $50 R_E$ wide magnetotail. The Earth frame E_z is given by $E_z = \gamma(E'_z - u_x B'_y)$, where γ is nearly 1.0 for any reasonable magnetotail convection speed.

As a result, E'_z differs significantly from E_z only when B_y is nonzero. A relatively large u_x is obtained by picking $E_{y0} = 0.3$ mV/m and $B_{z0} = 3$ nT, yielding $u_x = 100$ km/s. If, for example, $B_{y0} = -1$ nT, then the resulting difference between E_z and E'_z is $\gamma u_x B_{y0} = 0.1$ mV/m. Even though the above figures show that E_z can be substantially different in the two frames when $B_{y0} \neq 0$, the changes in E_y and E_z between the two frames leave $\mathbf{E} \cdot \mathbf{B}$ invariant. Both observers therefore see the parallel acceleration of electrons that is required to maintain charge neutrality.

Alekseyev and Kropotkin [1970] considered particle orbits near an infinitely thin current sheet, and *Cowley* [1978] used the constancy of P'_x when $B_{y0} = 0$, to show that the guiding center of a particle leaves the current sheet a distance

$$\Delta y = y_2 - y_1 = \frac{v|B_x|}{\Omega_{z0} B} [|\cos\alpha_1| + |\cos\alpha_2|] \quad (7)$$

in the cross-tail direction from the point the particle entered the current sheet. In (7), $|B_x|$ and B are assumed to be the same at the entry and exit points, and α is the pitch angle. Repeating Cowley's derivation for the one-dimensional plasma sheet with $B_{y0} \neq 0$ yields

$$\Delta y = \frac{(v_{x2} - v_{x1}) + \Omega_{y0} (z_2 - z_1)}{\Omega_{z0}} \quad (8)$$

for the exact displacement of a single particle that enters the current sheet at z_1 with velocity v_{x1} and leaves at z_2 , v_{x2} . Averaging over phase angle gives the mean (or guiding center) Δy

$$\Delta y = \frac{v}{\Omega_{z0}} \left[\frac{|B_{x2} \cos\alpha_2|}{B_2} + \frac{|B_{x1} \cos\alpha_1|}{B_1} \right] + \frac{\Omega_{y0}}{\Omega_{z0}} (z_2 - z_1) \quad (9)$$

Equation (9) reduces to (7) if the entry and exit points are at the same z . However, the last term in (9), which also can be written as $B_{y0} (z_2 - z_1) / B_{z0}$, is large if a particle enters in one hemisphere (e.g., $z_1 > 0$) and leaves in the other hemisphere ($z_2 < 0$). As noted above, field lines do not lie in the x - z plane when $B_{y0} \neq 0$, so even a particle which exactly follows a field line enters and leaves the plasma sheet at substantially different y locations when it travels from one hemisphere to the

other.

The addition of B_{y0} and the resulting last term in (9) does not affect particle energization. Since $E'_y = 0$ in the moving frame, no energization is associated with motion in the y direction. In the Earth frame, $E_y \neq 0$ so the extra Δy in (9) that results from the addition of B_{y0} may appear to energize a particle that enters the current sheet from one hemisphere and leaves in the other. However, the previously discussed extra E_z term in the Earth reference frame ($\gamma u_x B_{y0}$), when multiplied by $(z_2 - z_1)$, cancels the energization due to the extra Δy effect, at least to the order $\gamma - 1$ considered here. As a result, the addition of B_{y0} does not affect particle energization in either the moving frame or the Earth frame. The above example points out the need to include both $q\Delta y E_y$ and $q\Delta z E_z$ when considering energization in the Earth frame when $B_{y0} \neq 0$ rather than simply assuming that the acceleration of a plasma sheet particle is proportional to Δy .

4. ORBITAL EFFECTS OF B_y : $N=1$ RESONANT ORBITS

The imposition of B_{y0} modifies both the dynamics and the current-carrying properties of plasma sheet ions. Here these two effects are analyzed separately for ions at the $\kappa = 0.53$ resonance.

Average Pitch Angle Changes

Figure 4 shows how the addition of B_{y0} changes the dynamical nature of ion orbits near the $N = 1$ resonance. Between 100 and 300 groups of 100 protons each were followed to produce this and each of the other contour plots in this paper. Particles in any one group had the same energy W and moved in a fixed field model, so all particles in a single group had the same κ . In Figure 4a $\langle \Delta\alpha \rangle$, the rms pitch angle change, was evaluated using the untrapped ions in each group. All ions were injected from the northern hemisphere, so that the initial pitch angle $\alpha_i > 90^\circ$. The quantity $\Delta\alpha$ was defined as $|\alpha_i - \alpha_f|$ for ions that left the current sheet in the southern hemisphere so that the final pitch angle $\alpha_f > 90^\circ$. The quantity $\Delta\alpha$ was defined as $|180^\circ - \alpha_i - \alpha_f|$ for ions that left in the northern hemisphere so that $\alpha_f < 90^\circ$. With this definition $\Delta\alpha = 0^\circ$ if an ion which began with

$\alpha_i = 170^\circ$ left with α_f either 10° or 170° . This, and most of the following plots, are labeled by proton energy in a given model field rather than by the κ parameter so they could more easily be related to observations. Ions with $W = 1, 2.8,$ and 5 keV have $\kappa = 0.69, 0.53,$ and 0.46 respectively. The other magnetic field parameters are fixed at $B_{x0} = 32$ nT, $B_{z0} = 3.3$ nT, and $L = 1.0 R_E$ for all groups. Figure 4a shows that $\langle \Delta\alpha \rangle$ is less than 5° at the resonant energy of 2.8 keV when $B_{y0} = 0$. One of the most striking observations of this work is that the region of small $\langle \Delta\alpha \rangle$, which is characteristic of resonant orbits, completely vanishes by the time $|B_{y0}|$ reaches 0.5 nT. The average pitch angle change is between 25° and 30° for all energies in this initially isotropic ($T_{\parallel}/T_{\perp} = 1$) distribution when $0.5 \text{ nT} < |B_{y0}| < 3 \text{ nT}$. In this range of $|B_{y0}|$, no evidence of compensated or resonant orbits appears at any of the energies shown in Figure 4. The second region of small $\langle \Delta\alpha \rangle$, at large negative B_{y0} , is discussed below. It should be noted that large $\langle \Delta\alpha \rangle$ does not necessarily mean that there is a poor correlation between α_f and α_i . A large $\langle \Delta\alpha \rangle$ often is produced by a systematic difference between these two angles, as discussed in Section 6.

Figure 4b is a contour plot of R , the fraction of untrapped ions that both entered and left the plasma sheet in the northern hemisphere. Resonant 2.8 keV ions essentially all crossed the $x = 0$ plane twice when $B_{y0} = 0$. The ions appeared to simply bounce off or were all reflected by the current sheet, giving $R = 1$. When B_{y0} was strong and negative the ions were guided directly through the current sheet with almost no net change in μ or α ($R = 0$). A sample orbit illustrating this behavior is presented in the following section.

When B_{y0} was strong and positive, ions injected at $z > 0$ usually mirrored several times before leaving the modeling region. Orbits were stochastic, with μ and α changing erratically by a large amount each time the ion moved across the current sheet from north to south. Ions usually mirrored in the southern hemisphere and then returned to cross the current sheet from south to north. For this south-to-north crossing in a field with large positive B_{y0} the ions behaved the same as ions did when they crossed from north to south with a strong negative B_{y0} , i.e. α and μ were

almost unchanged. Ions therefore would mirror next in the northern hemisphere with almost the same trajectory they had just followed in the southern hemisphere. This sequence of mirroring at random locations in the southern hemisphere followed by an almost identical orbit in the northern hemisphere would continue until a particle happened to leave the southern side of the current sheet with a small enough pitch angle to escape. Figure 4b therefore shows that essentially all ions which escaped when $B_{y0} = +5$ nT did so in the southern hemisphere ($R = 0$).

Individual Orbits and $\langle v_y \rangle$

Rather than the many groups of several hundred protons each that were used to prepare Figures 2 and 4, Figure 5 shows the orbit of a single 3-keV proton. One ion was injected at $z = 1 R_E$ with the same pitch and phase angles ($\alpha = 160^\circ$, $\psi = 90^\circ$) into fields which differed only in the value of B_{y0} . Other parameters were the same as in Figure 4. The radius of the spiral, and therefore α and μ , were almost the same when the ion entered and left the current sheet in the $B_{y0} = 0$ panel. The final spiral radius, μ , and α are substantially different in the $B_{y0} = -0.2$ nT panel. The proton barely escaped after a single neutral sheet interaction, with α near 90° , when $B_{y0} = -0.4$ nT. The proton mirrored one or more times within the current sheet in each of the lower 3 panels. The resulting final α is almost arbitrary in these latter cases, yielding a large $\Delta\alpha$.

Even though μ and α changed substantially for $|B_{y0}|$ as small as several tenths of a nanotesla, the overall character of the orbit does not appear to have changed drastically in the top 3 panels. This suggests that the current-carrying properties, in which we are most interested, may not be quite so strongly dependent on B_{y0} .

Figure 6 shows the maximum $\langle v_y \rangle / v_o$, which usually is found near $z = 0$ (see Figure 2). This contour plot is based on the same orbits that were used to prepare Figure 4. The $\langle v_y \rangle / v_o$ parameter still shows a weak increase at 2.8 keV when $|B_{y0}| = 0.5$ nT. The strong guiding action of a very large negative B_{y0} again is evident, with $\langle v_y \rangle / v_o$ exceeding 0.8 at $B_{y0} = -5$ nT.

Figure 7 shows that the z dependence of $\langle v_y \rangle / v_o$ does not change drastically at the 2.8-keV

resonance energy when $|B_{y0}| < 0.4$ nT. This figure was prepared by tracing a group of 1000 protons in each of the 6 field models with different B_{y0} . Similar results were reported and discussed for the $B_{y0} = 0$ case in paper 2, and by *Ashour-Abdalla et al.* [1992b] using a two-dimensional magnetic field model. The magnitude of $\langle v_y \rangle / v_o$ decreased, and the peak became slightly more confined near $z = 0$ as $|B_{y0}|$ increased. The peak in $j_y(z)$ near but not exactly at $z = 0$, which is characteristic of resonant orbits, almost vanished when B_{y0} reached -1 nT. The $j_y(z)$ profile at $B_{y0} = -1$ nT in Figure 7 is more like a $B_{y0} = 0$ profile dominated by stochastic orbits ($\kappa = 0.40, 0.82$) than by resonant orbits (Figure 2).

5. ORBITAL EFFECTS AT HIGHER RESONANCES

N = 2 Resonant Orbits

Figure 8 shows that the situation is markedly different when W is increased to 23 keV, the $N = 2$ or $\kappa = 0.32$ resonance, in this same magnetic field. Even- N orbits involve an integer number of full sinusoidal oscillations during each current sheet interaction. An $N = 2$ ion that enters the current sheet from the northern outer CPS crosses the $z = 0$ plane 3 times, and leaves the current sheet to enter the southern outer CPS. The ions in Figure 8 came from an initial distribution with $T_{\parallel}/T_{\perp} = 10$ at the edge of the current sheet. Resonant effects in $\langle \Delta\alpha \rangle$ were present, but much less dramatic, when a $T_{\parallel}/T_{\perp} = 1$ distribution was used. Figure 8 shows that there is a striking difference between the effects of positive and negative B_{y0} on even- N orbits [*Dusenbery et al.*, 1993].

Figure 9 shows trajectories of two particles injected in the northern hemisphere. Ions generally drift in the positive y direction in the current sheet. For large $|B_{y0}|$, it is possible to find the symmetric trajectories that are needed to yield small $\langle \Delta\alpha \rangle$ only when $B_{y0} < 0$. Ions injected from the southern hemisphere have small $\langle \Delta\alpha \rangle$ when B_{y0} is large and positive. Figure 9 also shows how large the cross-tail motion is in a small region near $z = 0$ when B_{y0} is strong and negative. When $B_{y0} = -5$ nT, even the $N = 1$ ($\kappa = 0.53$) resonant particles, which were reflected from the

current sheet when $B_{y0} = 0$, are guided directly through the current sheet (Figure 4b). This is the region with very large $\langle v_y \rangle / v_o$ in Figure 6. In the $B_{y0} = -5$ nT field these $\kappa = 0.53$ particles have trajectories that look very similar to the $B_{y0} = -2$ nT orbit in Figure 9. A modest decrease in $\langle \Delta\alpha \rangle$ also is evident near the point at which $B_{y0} = 3.7$ nT in Figure 8. This structure is near the point at which $B_{y0} = B_{z0}$. However, an examination of individual orbits did not reveal any simple pattern such as those seen in the regions with very small $\langle \Delta\alpha \rangle$.

N = 3 Resonant Orbits

Figure 10 shows the $N = 3$ or $\kappa = 0.23$ resonance at $W = 3.6$ keV. This figure used $B_{x0} = 32$ nT, $B_{z0} = 3.3$ nT, $L = 0.2 R_E$, and $T_{\parallel}/T_{\perp} = 10$. The region of very small $\langle \Delta\alpha \rangle$ disappears at a few tenths of one nanotesla (Figure 10a). The $N = 2$ resonance is at $W = 900$ eV in this magnetic field. Figure 10a again illustrates that $\langle \Delta\alpha \rangle$ is strongly dependent on the sign of B_y at even- N resonances and nearly independent of the sign when N is odd.

Figure 10b shows that the resonant structure is present, but relatively weak in its effect on cross-tail currents or $\langle v_y \rangle / v_o$. This ratio exceeds 0.4 near $B_{y0} = 0$ at both the $N = 2$ and $N = 3$ resonances and drops below 0.2 half way between the resonances, near 2 keV. The guiding action of very strong B_{y0} fields, illustrated in Figure 9, again produces much larger values of $\langle v_y \rangle / v_o$ at $B_{y0} = -2$ nT than at $B_{y0} = 2$ nT for these particles that were injected in the northern hemisphere.

N = 6 and 7 Nonresonant Orbits

Figure 11 shows that weak periodic structure can be detected near and even beyond $\kappa = \kappa_r$. In Figure 11, which used $B_{x0} = 32$ nT, $B_{z0} = 3.3$ nT, and $L = 0.04 R_E$, κ decreases from 0.14 at $W = 1$ keV to 0.088 at $W = 6$ keV, while $\kappa_r = 0.10$. Even though there are no regions of very small or very large $\langle \Delta\alpha \rangle$, weak minima are evident when $B_{y0} = 0$ at 1.8 keV ($N = 6$ or $\kappa = 0.12$) and at 3.4 keV ($N = 7$ or $\kappa = 0.10$). Figure 11 was prepared using $T_{\parallel}/T_{\perp} = 10$ to emphasize the weak minima in $\langle \Delta\alpha \rangle$, which are almost absent in a $T_{\parallel}/T_{\perp} = 1$ distribution. It may be noted that the minima have shifted away from the locations predicted by (4) in this nonresonant region. The failure

of (4) to predict the exact locations of minimum $\langle \Delta\alpha \rangle$ for nonresonant orbits is not surprising because these ions can bounce beyond the edge of the current sheet ($|z| = L$) during the meandering portion of each orbit. The κ parameter was defined [Büchner and Zelenyi, 1989] using a linear approximation for bounce frequencies and radii of curvature near $z = 0$ rather than for particles that bounce out into a region of nearly uniform field. At very small κ values, Büchner and Zelenyi [1989] showed that a normalized form of I_z is more important than κ in determining pitch angle diffusion rates. The previously discussed dependence of $\langle \Delta\alpha \rangle$ on the sign of B_{y0} for odd and even N also can be seen in Figure 11. A plot of $\langle v_y \rangle / v_o$ showed essentially no dependence on W or κ even when $T_{\parallel} / T_{\perp} = 10$. Cross-tail currents therefore show essentially no periodic κ -dependence when $\kappa \leq \kappa_r$.

We have used (3) to define κ even when $B_{y0} \neq 0$. If κ^2 is defined as the ratio of the field line radius of curvature R_c to the maximum particle gyroradius, both evaluated at $z = 0$, then a second parameter

$$\kappa_{ns} = B_{z0} \left[\frac{Lq}{B_{x0}mv} \right]^{1/2} \left[1 + \frac{B_{y0}^2}{B_{z0}^2} \right]^{3/4} \quad (10)$$

[Karimabadi et al., 1990; Büchner and Zelenyi, 1991] also is important in determining orbital characteristics. The ratio κ_{ns} / κ is 1.07, 1.26, 1.57, 1.97, and 2.45 when $|B_{y0}| = 1, 2, 3, 4,$ and 5 nT respectively, with $B_{z0} = 3.3$ nT. Although phase space characteristics are dependent on κ_{ns} or $\kappa_s = \kappa (B_{y0} / B_{z0})$ [Büchner and Zelenyi, 1991], Figures 4, 8, 10, and 11 show that the locations of resonances are nearly independent of B_{y0} . When $\kappa > \kappa_r$, the energy of an ion at the N th resonance therefore is well predicted by (4), which involves κ but not κ_{ns} [Dusenbery et al., 1993].

6. LOW ALTITUDE SIGNATURES

Figure 12 compares pitch angle changes produced by two processes. The basic parameter set used was $B_{x0} = 32$ nT, $B_{y0} = 0$, $B_{z0} = 3.3$ nT, $L = 1.0 R_E$, and $W = 2.8$ keV. Either W or B_{y0} was changed to prepare panels *b*, *c*, and *d*, as noted below. Each marker shows the initial and final

pitch angles of one ion that started and ended at $|z| = 4L/3$. The parameter $(180^\circ - \alpha_i)$ was plotted on the x axis because orbits started in the northern hemisphere, where incoming ions have $\alpha_i > 90^\circ$. The y axis shows the final pitch angle, α_f . Figure 12a used the basic set of parameters, which placed ions near the $N = 1$ resonance (Figure 4). If compensation was exact for ions with all pitch and phase angles, then $(180^\circ - \alpha_i)$ and α_f would be equal. Figure 12a shows a narrow band of ions that very nearly satisfy this requirement for exact resonance. A second broader but still very sharply bounded distribution of final pitch angles is evident at large $(180^\circ - \alpha_i)$. At these pitch angles, $\Delta\alpha$ becomes phase angle dependent, with a well defined maximum $\Delta\alpha$.

Figure 12b shows the distribution of pitch angles for 3.5 keV ions, which are not near a resonance. Figure 4 shows that when $B_{y0} = 0$, the mean pitch angle change for a 3.5 keV proton is approximately 15° . Figure 12b presents more detailed pitch angle information for these ions. An initially field-aligned ion ($180^\circ - \alpha_i = 0^\circ$) leaves with $\alpha_f = 15^\circ$. The final pitch angles are distributed throughout a clearly bounded range for other α_i . A simplistic picture that can explain the sharp cutoffs in α_f for each α_i (paper 1) is that the net effect of a current sheet interaction is to deflect all incident ion velocity vectors as a block through the same scatter angle experienced by a field-aligned ion (15° in this case). This model would confine points in Figure 12b to a diagonal band with a height of 30° along the α_f axis. Figure 12b shows that this simple model fails to explain two features of the calculations. First, for $(180^\circ - \alpha_i) > 30^\circ$ the band of points exceeds the expected 30° range in α_f , even though the band retains its sharp edges. This again suggests that $\Delta\alpha$ has some phase angle dependence. In addition, the clustering of points in certain patterns within the allowed band is not explained.

It is not surprising that $\Delta\alpha$ shows some dependence on $(180^\circ - \alpha_i)$ when this latter angle becomes large. Many of the analytic results have been derived for limiting cases, such as small I_z and large or small κ . One striking feature of orbit tracing analyses is that resonances such as that at $\kappa = 0.53$ are so nearly independent of the injection pitch and phase angles [Büchner, 1991].

Savenkov et al. [1991] and *Brittnacher and Whipple* [1991] studied the phase angle dependence of changes in I_z . It was shown that I_z of generally field-aligned ions jumps by a predictable amount when the ion crosses the first separatrix, from spiraling to meandering motion. The jump in pitch angle during the second separatrix crossing (from meandering back to spiraling motion) is strongly dependent of the phase angle of the incident ion. Changes in I_z or pitch angle vary smoothly with phase angle, but at certain critical phase angles ΔI_z becomes especially sensitive to the incident conditions. This behavior may explain the internal banding structure that is evident in Figures 12a and 12b.

The $W = 5.5$ keV protons in Figure 12c are farther from the resonance, so an initially field-aligned ion leaves the current sheet with $\alpha_f = 52^\circ$. The pattern out to $(180^\circ - \alpha_i) = 10^\circ$ is approximately described by a shift of all ion directions by 52° . In Figure 11c, some protons with $(180^\circ - \alpha_i) > 10^\circ$ have α_f very widely distributed. This behavior begins when the sharply bounded range of α_f reaches 90° . At this point, ions begin to mirror within the current sheet rather than escaping after one current sheet encounter. These ions essentially are reinjected with much different pitch angles. Protons with $\alpha_f > 90^\circ$ in Figure 11c left the current sheet in the southern hemisphere.

Figure 12d was made by injecting the same 2.8-keV ions as in panel a into a field with $B_{y0} = -0.2$ nT. Figure 4a shows that both the $(B_{y0} = 0, W = 3.5$ keV) and the $(B_{y0} = -0.2$ nT, $W = 2.8$ keV) points lie on the $\langle \Delta \alpha \rangle = 15^\circ$ contour. A comparison of Figures 12b and 12d shows that moving away from the $(B_{y0} = 0, W = 2.8$ keV) resonance point either by shifting W or by shifting B_{y0} produces very similar pitch angle distributions near odd- N resonances. However, it should be recalled that odd- N resonances appear only when $B_{y0} = 0$. It is not possible to return to an odd- N resonance by changing W in a non-zero B_{y0} . *Büchner and Zelenyi* [1991] previously compared changes in surface of section plots, and therefore in the type of orbit followed by an ion, that are produced by separately varying κ and κ_s . This is equivalent to our changes of W and B_{y0} .

It has been shown that low altitude satellites can detect ions in a broad energy range which precipitate from regions of the plasma sheet that are dominated by stochastic orbits [Ashour-Abdalla *et al.*, 1992a; Bosqued *et al.*, 1993]. A gap in which ion precipitation diminished also was seen at low altitude. The gap was attributed to a wall or Alfvén-layer-like region at which $\kappa \approx 1$ that is associated with rapid drift across the tail (in a two-dimensional model) or around the Earth (in a three-dimensional model). Finally, it was suggested that groups of ions may be strongly accelerated near the neutral line to form beamlets, which also could be detected at low altitudes.

We suggested in paper 1 that it may be possible to detect a different resonant orbit effect that would be observable only in very narrow energy bands. Some energy can be found at which particles are resonant on almost any midtail field line. The requirement for the low altitude observation of a very narrow-banded feature is that field-aligned ions must suffer less than a 1° change in pitch angle as they pass through the current sheet. One consequence is that the loss cone will remain empty when equatorial pitch angles change by $< 1^\circ$. Our finding that odd- N resonances completely disappear when a small B_{y0} is added suggests that the proposed effect will not exist at odd- N resonances. However, very small pitch angle changes are possible at even- N resonances, so the proposed effect is investigated further here.

Since we are interested only in ions that reach low altitude satellites, a highly field-aligned distribution ($T_{\parallel}/T_{\perp} = 10^4$) was injected at $z = L$ to prepare Figure 13. The field parameters were $B_{x0} = 32$ nT, $B_{z0} = 3.3$ nT, and $L = 0.4 R_E$. When $B_{y0} = 0$, ions in an 0.1 keV wide energy band at the $N = 2$ resonance (3.66 keV) left the current sheet with less than 1° rms pitch angle changes. Figure 13 shows that a region with $\langle \Delta\alpha \rangle < 1^\circ$ remains when B_{y0} becomes large. In fact, the energy band in which $\langle \Delta\alpha \rangle < 1^\circ$ becomes 2 or 3 times wider at the larger B_{y0} values shown, suggesting that the effect might be easier to detect at low altitudes when B_{y0} is large. Figure 13 again shows that the resonant energy depends only weakly upon B_{y0} .

If a resonant energy could be detected at low or middle altitudes, it would provide a way to

measure the ratio $B_{z0}^2 L / B_{x0}$ appropriate to the Harris model at the equatorial end of the field line. Either of two specific effects may be observable. At any location, ions in the very narrow resonant energy bands would not be scattered enough to fill the usual upgoing loss cone. A downgoing loss cone therefore would exist, and could be seen at any middle or low altitude. Since downgoing ion fluxes generally are weak, it would be difficult to identify such a narrow band feature. However, intense upgoing ion beams are often observed. The lack of any pitch angle change in the current sheet would result in a very narrow energy downgoing ion beam. Ions at adjacent nonresonant energies would be scattered to form an isotropic rather than a beam-like downgoing distribution at low and middle altitudes.

7. BIRKELAND CURRENT GENERATION

Overview

This section uses the arguments proposed by *Vasyliunas* [1972] to connect cross-field drift and field-aligned current [*Siscoe and Maynard*, 1991; *Heinemann and Pontius*, 1991; *Pontius*, 1992; and *Birmingham*, 1992]. The original analysis was based on the experimental observation that electrons carry nearly all the field-aligned current. This is true even within ion beams [e.g., *Kaufmann and Kintner*, 1984]. As a consequence, the ion continuity equation

$$\nabla \cdot [q_i N_i (\mathbf{V}_B + \mathbf{V}_{di})] = -\partial (q_i N_i) / \partial t \quad (11)$$

requires that equal ion fluxes drift in and out the sides of a stationary flux tube during steady-state conditions. In (11), $N_i = N_e = N$ is the number of ions and of electrons in a flux tube with unit cross section at the ionospheric end. The $\mathbf{E} \times \mathbf{B}$ drift velocity \mathbf{V}_B is the same for ions and electrons. Both \mathbf{V}_B and \mathbf{V}_{di} , the sum of all other ion guiding center drift velocities, are referenced to the ionosphere.

A substantial net electron flux is permitted to drift through the sides of a stationary flux tube. Electron continuity is satisfied by electrons flowing into or out of the ionosphere through the end of the flux tube

$$\nabla \cdot [q_e N_e (\mathbf{V}_B + \mathbf{V}_{de})] = -\partial (q_e N_e) / \partial t - j_{\parallel} \quad (12)$$

where the electron q_e is negative, and positive Birkeland current j_{\parallel} flows down to the ionosphere. We will consider only steady-state conditions in the remainder of this work, so $\partial (qN) / \partial t = 0$. Since the average ion is substantially more energetic than the average electron, \mathbf{V}_{de} often is neglected relative to \mathbf{V}_{di} and \mathbf{V}_B in the guiding center treatment.

The above expressions show that the underlying cause of field-aligned current is that the derivatives of $N_e \mathbf{V}_{de}$ and $N_i \mathbf{V}_{di}$ are different, but that $N_e = N_i$. In general, any difference between variations in fluxes resulting from ion and electron drift requires the presence of Birkeland current to maintain charge neutrality. We assume that any parallel electric fields that are needed to maintain $N_e = N_i$ will form and either precipitate magnetospheric electrons or extract ionospheric electrons.

In the present study, average drift velocities were calculated only inside the magnetotail current sheet. We therefore divide each flux tube into two segments. The current sheet segment is defined as extending between the $z = 0$ and $z = L$ planes, where drift velocities have been calculated. Beyond this point $\mathbf{V}_{de} = \mathbf{V}_{di} = 0$ in our one-dimensional model, though these drifts will be nonzero in a three-dimensional model. The flux tube is chosen to have a rectangular cross section at $z = 0$. The remainder of the flux tube extends from $z = L$ to the ionosphere. This magnetospheric segment of the flux tube is selected to have a unit area at its ionospheric end. The guiding center approximations and the previous analyses are valid in the magnetospheric segment, except for the addition of current through the end at $z = L$.

Current continuity and charge neutrality are maintained in the current sheet segment by considering drift through the 4 sides of a flux tube and drift plus Birkeland current through the end at $z = L$. By symmetry, no current flows through the end at $z = 0$. Current flowing out the $z = L$ end of the current sheet segment flows into the magnetospheric segment. Part of this current serves as an additional source to the usual guiding center analysis, and therefore adds to the current which

must reach the ionosphere. The analysis would be simpler if flux tube segments were defined with ends that are normal to \mathbf{B} , but our calculations are all based on boxes aligned in the x , y , and z directions. It may be noted that $\mathbf{E} \times \mathbf{B}$ drift produces equal electron and ion fluxes, and no net current through the faces of the two segments at $z = L$. Neglecting the $\mathbf{E} \times \mathbf{B}$ drift contribution to currents through these two $z = L$ faces will not change the basic conclusions regarding Birkeland current flowing to the ionosphere. Since non-guiding-center aspects of particle motion are important only in the current sheet segment, this is the only segment that is considered in the remainder of this section.

Elementary Models

Figures 2 and 7, as well as several figures in paper 2, show that when $\mathbf{E} = 0$ a resonant ion has a much larger $\langle v_y \rangle$ than does a stochastic ion. This is true both for the peak $\langle v_y \rangle$ and also for the average v_y integrated through the current sheet. Electrons follow guiding center motion in this region. It is the difference between variations of the cross-tail drifts of guiding center electrons and of both resonant and stochastic ions that tends to create the charge imbalance that is studied here. The treatment in the present section differs from previous guiding center drift analyses through this emphasis on the abrupt changes in $\langle v_y \rangle$ that can be produced near resonances by modest changes in magnetic field parameters.

Figure 14 illustrates the proposed mechanism. Both the original T89 model that was used in paper 1 and the version of T89 that was modified by *Pulkkinen et al.* [1992] in order to reproduce satellite observations during specific substorms showed that constant- κ contours are curved in the sense shown by the solid curves near the Earth in Figure 14. The κ labels used by Pulkkinen et al. are for electrons, but contours of ion κ have the same shapes. The particular contours shown in Figure 14a were selected because ions are stochastic at $\kappa = 0.82$ and resonant at $\kappa = 0.53$.

The heavier and lighter arrows showing V_{di} at $\kappa = 0.53$ and at $\kappa = 0.82$ in Figure 14a are intended to indicate variations in cross-tail drift speed. Ions do not appear, disappear, or even

change their energy when viewed in the moving coordinate system of our one-dimensional model field, but simply change their average cross-tail drift velocities when they pass between resonant and stochastic regions.

To provide the simplest model that can illustrate the effects of interest, we consider a region in which the magnetic field varies as one moves in the y and z directions, but is independent of x . We selected an electric field E_y that is independent of y within the flux tube, but that may vary in x . The sketches all assume that \mathbf{V}_B is exactly in the x direction at $z = 0$ and that \mathbf{V}_d is in the y direction.

Figure 15a shows particle fluxes flowing through the sides of a rectangular flux tube that extends from the ion $\kappa = 0.82$ contour on the left to the $\kappa = 0.53$ contour on the right. This orientation corresponds to the dusk ($y > 0$) side of Figure 14a. Figure 15a is appropriate for a region containing a uniform E_y and N that varies only in the y direction. Equal fluxes NV_B of ions are shown drifting into the tailward side and out of the earthward side of the tube. Since V_{di} is larger on the right side than on the left side of Figure 15a, the illustrated density gradient in the y direction is required in order to satisfy ion continuity (11).

Electrons drift earthward at the same speed and have the same density as ions, so the electron fluxes flowing into the tailward edge and out of the earthward edge also are equal in Figure 15a. Since the guiding center electron drift does not change rapidly in the y direction, more electrons will drift in from the side with higher density than drift out the side with lower density. An electric field must form so that the excess electrons will flow into the magnetospheric segment of the flux tube, contributing to an upward j_{\parallel} .

Current continuity also could be satisfied with the same \mathbf{B} and perpendicular \mathbf{E} fields used in Figure 15a by assuming that the density gradient is in the positive x direction. Ion and electron fluxes and drift velocities in this case are sketched in Figure 15b. The uniform V_B requires more electrons and ions to leave the earthward side of the flux tube where the density is high than enter

the tailward side. The ion continuity requirement (11) could sometimes be satisfied with no density gradient in the y direction because ions drift more rapidly when they enter the dawn side of the flux tube than when they leave through the dusk side. Since V_{de} is uniform, there is a net outward flux of electrons through the sides of the flux tube, which must be balanced by electrons that enter through the end at $z = L$. This contributes to a downward j_{\parallel} in the magnetospheric segment of the flux tube.

As a final simple example, all the fluxes sketched in Figure 15b can be obtained with N completely uniform if E_y increases as one moves in the earthward direction. An x -dependence of E_y can produce the same change in NV_B as does an x -dependence of N . There clearly are many combinations of the elementary models sketched above that can satisfy (11) and (12) when V_{de} and V_{di} have different y -dependence. Almost all such models require Birkeland currents.

Figures 15c and 15d illustrate the same simple models applied to the dawn side of Figure 14a. Figures 15a and 15c both have the cross-tail and earthward ion drift currents separately satisfying the steady-state continuity equation. All Birkeland current is generated by the change in cross-tail electron flux that is associated with the density and accompanying pressure gradient. Since V_{de} is relatively small, this model results in a modest field-aligned current density. It may be noted that Figure 5 of *Kaufmann et al.* [1993b], which is based on the T89 model, shows little y dependence of the cross-tail current after integrating through the thickness of the current sheet.

In contrast, cross-tail and earthward ion currents each vary in Figures 15b and 15d. Equation (11) is satisfied because the two components of the divergence cancel. In this case Birkeland current arises because of the change in NV_B , the earthward electron drift flux. This change in NV_B can be produced either by an x -dependence in E_y or a gradient of N in the x direction. Since V_{di} is large, the change in NV_{di} and therefore of NV_B and j_{\parallel} in Figures 15b and 15d may be large. Note that Figures 15b and 15d require different gradients in N or E_y on the dawn and dusk sides. The product NV_B must increase earthward on the dusk side and must simultaneously increase tailward

on the dawn side of the magnetotail. As one example, this situation is possible even if N is uniform and the total cross-tail potential drop is independent of x . In this case, the region of strongest E_y would have to shift from the dusk side to the dawn side as one moved out the tail to be consistent with Figures 15b and 15d.

Current Magnitudes

The magnitudes of the fluxes described above can be estimated to see if it is reasonable to drive a significant night side steady-state Birkeland current solely from the magnetotail current sheet. *Iijima and Potemra* [1978] found that the average ionospheric j_{\parallel} is approximately $1 \mu\text{A}/\text{m}^2$. With $B = 50,000 \text{ nT}$ in the ionosphere and $B_{zo} = 5 \text{ nT}$ in the equatorial plane, a (not necessarily rectangular) 1 m^2 area in the ionosphere projects to a square box, similar to those sketched in Figure 15, with $a = 100 \text{ m}$ sides. Assuming an average number density of $n = 0.3 \text{ cm}^{-3}$ in the central plasma sheet [*Baumjohann et al.*, 1989] and a current sheet with half-thickness of $h = 1 R_E$ yields a flux of $nha\langle v_{di} \rangle = 2 \times 10^{14} \langle v_{di} \rangle$ ions/s passing through the left and right sides of the flux tube. The quantity $\langle v_{di} \rangle$ is $v_y(z)$ averaged through the current sheet for the geometry in Figure 15. Using the model in Figure 15b as an example, the rate at which ions accumulate in the flux tube owing to cross-tail drift is $2 \times 10^{14} a (d\langle v_{di} \rangle / dy) = 2 \times 10^{16} (d\langle v_{di} \rangle / dy)$ ions/s. As discussed above, Figure 15b shows a net loss of both ions and electrons through the other two sides at this same rate owing to $\mathbf{E} \times \mathbf{B}$ drift. The net effect is for the electron content of the flux tube to decrease at a rate of $2 \times 10^{16} d\langle v_{di} \rangle / dy$ electrons/s. The corresponding expression for the model in Figure 15a can be written as $2 \times 10^{16} (\langle v_{de} \rangle / \langle v_{di} \rangle) d\langle v_{di} \rangle / dy$ electrons/s. An ionospheric j_{\parallel} of $1 \mu\text{A}/\text{m}^2$ requires 6×10^{12} electrons/s flowing up from the ionosphere through the end of the flux tube. The value of $d\langle v_{di} \rangle / dy$ required in Figure 15b for steady state therefore is $3 \times 10^{-4} \text{ (m/s)/m}$ or $2 \text{ (km/s)/}R_E$. In Figure 15a $d\langle v_{di} \rangle / dy$ must be $(\langle v_{di} \rangle / \langle v_{de} \rangle)$ times larger.

To see if the above $d\langle v_{di} \rangle / dy$ estimates are reasonable, note that Ampere's law requires a total cross-tail current, integrated through the current sheet thickness, of $K_y = 32 \text{ mA/m}$ if B_x is

20 nT on one side of the current sheet and -20 nT on the other side. Assuming that most cross-tail current is carried by ions, this $K_y \approx 2enh\langle v_{di} \rangle$ requires $\langle v_{di} \rangle \approx 50$ km/s using the same density and half-thickness as before. The above estimates therefore show that $\langle v_{di} \rangle$ in Figure 15b must change by several percent per Earth radius of displacement in the y direction to supply all the electrons needed for a $1 \mu\text{A}/\text{m}^2$ ionospheric Birkeland current.

Drift Paths

We traced several ion groups in the full three-dimensional T89 $K_p = 4$ magnetosphere model. The purpose was to see if $\langle v_{di} \rangle \cdot \nabla \kappa$ is large enough so that most ions would drift from regions with $\kappa = 0.40$ to 0.53 or from 0.53 to 0.82 before reaching the flanks. We chose $\mathbf{E} = 0$ to isolate cross-tail drift from $\mathbf{E} \times \mathbf{B}$ drift effects, and from the changes in κ due to particle energization. The use of $\mathbf{E} = 0$ also simplifies the analysis by making it unnecessary to evaluate $\mathbf{E} \times \mathbf{B}$ drift through the boundary between the current sheet and magnetospheric segments of a flux tube. Note that the model in Figures 15a and 15c can be drawn with $\mathbf{E} = 0$ and therefore $NV_B = 0$.

A group of 5 keV protons was injected at $x = -20 R_E$, $y = z = 0$ in the T89 model to produce Figure 16. The κ parameter was calculated each time an ion crossed the equator. The κ parameter was defined as $(R_c / \rho_z)^{1/2}$ where R_c , the field line radius of curvature, was calculated using $R_c / R_c^2 = -(\mathbf{B} \cdot \nabla) \mathbf{B} / B^2$ at each equatorial plane crossing and $\rho_z = mv / eB_z$ was evaluated at $z = 0$. Since $\mathbf{E} = 0$, W and v are constant, and changes in κ are produced by drift to regions with different equatorial B_z and different R_c .

Figure 16a is a plot of equatorial crossing points, and shows that $\langle v_{di} \rangle$ was primarily in the cross-tail direction for $|y| < 10 R_E$. Drift paths became more nearly circular, centered at the Earth, beyond $|y| = 10 R_E$, so a comparison with one-dimensional results becomes less meaningful here. Figure 16b shows how κ changed as the ions moved across the tail. This group of ions moved approximately $3.5 R_E$ in the y direction to go from $\kappa = 0.53$ to $\kappa = 0.82$. These results are similar to those shown in *Pulkkinen et al.* [1992] and paper 1. The $d\langle v_{di} \rangle / dy$ of 2 (km/s)/ R_E needed to

generate $j_{\parallel} = 1 \mu\text{A}/\text{m}^2$ therefore requires a 15% change in $\langle v_{di} \rangle$ between the $\kappa = 0.53$ and $\kappa = 0.82$ contours. A change of this magnitude appears reasonable from our one-dimensional analysis (e.g. Figure 2), but a full three-dimensional calculation will be required before definitive conclusions can be drawn. At present, the suggestion that significant field-aligned currents are associated with cross-tail drift between regions dominated by stochastic orbits and regions dominated by resonant or guiding center orbits must be considered speculative.

8. CONCLUSIONS

Odd-N Resonances

It was shown that the addition of a uniform cross-tail magnetic field, which is comparable to that typically measured in the magnetotail, completely eliminated the resonances that exist when $B_{y0} = 0$ for particles that left the current sheet on the same side from which they entered. Pitch angle changes were found to depend especially sensitively on B_{y0} near these odd- N resonances. As a result, all ions that flow up from the ionosphere with energies that place them either near an odd- N resonance or in a stochastic region between resonances will suffer large pitch angle changes in the typical current sheet. Upgoing beams of all such ions will be so strongly deflected at the equator that they will not appear beam-like after a single current sheet interaction. Similarly, an empty loss cone in an upgoing distribution of such ions will be filled during each interaction with the current sheet. The electric current carried by odd- N resonant ions was found to depend a little less sensitively upon B_{y0} than did the average pitch angle change.

Even-N Resonances

Ions were found to behave differently near even- N resonances. Orbits can remain more symmetric at these energies (Figure 9b), so that resonant behavior is not so strongly affected by the addition or removal of a typical B_{y0} (Figures 8 and 10). Narrow energy bands were found in which only very small pitch angle changes took place during an even- N resonant current sheet interaction (Figure 13). Ions near these resonances suffer little scattering when they enter the cur-

rent sheet from the northern hemisphere and leave in the southern hemisphere if $B_{y0} < 0$. Particles going the other way through the current sheet suffer little scattering when $B_{y0} > 0$. Unscattered ions can be recognized at low or middle altitudes by the presence of downgoing loss cones (loss cones that have not been filled in during traversal of the current sheet) or by the presence of downgoing ion beams (upgoing beams which have passed through the current sheet). These features will be restricted to very narrow energy ranges. Detection of either signature at low or middle altitudes should provide information about the equatorial magnetic field structure. Since cross-tail current depends less strongly upon B_{y0} than does pitch angle scattering, the structure of the current sheet appears to be changed only modestly by the addition of a typical B_{y0} near an even- N resonance.

Cross-Tail and Field-Aligned Currents

The study of currents carried by individual charged particles provided new insight into possible causes of some steady-state Birkeland currents. The feature that is required for operation of the proposed mechanism to drive field-aligned currents is for cross-tail drift to carry ions across contours of constant κ . When $\langle \mathbf{v}_{di} \rangle \cdot \nabla \kappa$ is nonzero in the near-Earth plasma sheet, i.e. when contours of constant κ are curved as in Figure 14, then ions drift between regions characterized by different dominant orbit types. The lowest altitude resonant and stochastic regions are most important because there is a large energy separation between ions at adjacent resonances (Figures 2, 4, and 8). The large energy separation permits most ions in a Maxwellian distribution to follow resonant orbits at one location in the tail, and to follow stochastic orbits at a different y .

One-dimensional orbit calculations showed substantial changes in the average drift speed during the transition between points characterized by $\kappa = 0.53$ and by $\kappa = 0.82$ when $B_{y0} = 0$. When B_{y0} is substantial, the first resonant transition is that between $\kappa = 0.32$ and $\kappa = 0.40$. Similar changes also exist at the $\kappa > 1.5$ guiding center to $\kappa = 0.82$ stochastic transition. These are the points at which integral ion densities and pressures may change, and at which Birkeland currents

may be needed to maintain charge neutrality. We have not carried out the three-dimensional calculations that would be needed to compare the proposed mechanism to results from the usual guiding center analysis.

The calculations assumed that the same flux of ions drifts into and out of the sides of a stationary magnetic flux tube. This assumption is commonly used because field-aligned currents are observed to be carried predominantly by electrons. Ions do not enter or leave the plasma sheet, but merely drift faster or slower as κ changes. The other standard assumption is that the plasma is neutral. Since electrons follow guiding center motion in this magnetotail region, their drift velocity does not change abruptly near an ion resonance. As a result, the electron flux entering the sides of the magnetic flux tube does not equal the flux leaving the tube. The difference must be supplied by electrons entering from or precipitating into the ionosphere through the tube ends. The possibilities that electrons accumulate primarily through changes in the cross-tail fluxes (Figures 15a and 15c) and through changes in the flux associated with earthward $\mathbf{E} \times \mathbf{B}$ drift (Figures 15b and 15d) both were considered. In either case, electrons carry the current that is diverted to the ionosphere, even though ions carry most of the cross-tail current. Since a specific flux of electrons is required to maintain neutrality, the proposed mechanism operates as a current generator rather than a voltage generator. Parallel voltage drops must form, but their magnitudes will be whatever is needed to drive the required j_{\parallel} .

The present analysis does not address the question of why constant κ surfaces are curved as they are in the standard magnetic field models, and only steady-state conditions were investigated in this work. The ionosphere and its response to imposed currents are critical, especially when temporal effects are considered. These essential but very complex aspects of the Birkeland current system have not been addressed in the present work.

It should be noted that the abrupt changes in $\langle v_{di} \rangle$ predicted near ion resonances by orbit tracing studies will not appear in simulations that use MHD or the guiding center equations. The pro-

posed Birkeland currents should appear in any kinetic simulation that bases electric currents on the actual motion of individual particles, even if orbit tracing is relatively crude. In this regard, the present analysis may be compared with the interesting conclusion of *Wolf and Pontius* [1993] that in certain circumstances the drift of non-guiding-center particles, when averaged throughout a flux tube, is the same as the drift that would be calculated using the guiding center equations. Their analysis is based on the assumption that the distribution function can be written as a function of only W and P_y , which are constants of the motion. The total energy W is constant in the steady state analyses that we consider, and it was noted in Section 3 that P_y is constant for one- and two-dimensional analyses. However, a requirement for variations of \mathbf{B} or \mathbf{E} in the y direction is inherent in any three-dimensional model that includes Birkeland currents associated with cross-tail drift resonances. As a result, P_y will not be a constant of the motion. Our one-dimensional analysis (paper 2) showed that the required self-consistent $f(\mathbf{v})$ is strongly dependent on variables other than W and P_y or v_y . More realistic two-dimensional analyses show a substantial x, z off-diagonal component of the pressure tensor [*Burkhart et al.*, 1992]. Further work clearly is needed before definitive conclusions can be drawn regarding the possible association between non-guiding-center motion and Birkeland current.

Acknowledgments. We would like to thank a referee who made many constructive comments. This material is based upon work supported by the National Science Foundation under grant ATM-92-02126 and by the National Aeronautics and Space Administration under grant ^{NAGW}~~NASA~~-1625.

REFERENCES

- Alekseyev, I. I., and A. P. Kropotkin, Interaction of energetic particles with the neutral sheet in the tail of the magnetosphere, *Geomag. and Aeronomy*, 10, 615-619, 1970.
- Ashour-Abdalla, M., L. M. Zelenyi, J. M. Bosqued, and R. A. Kovrazhkin, Precipitation of fast ion beams from the plasma sheet boundary layer, *Geophys. Res. Lett.*, 19, 617-620, 1992a.
- Ashour-Abdalla, M., L. M. Zelenyi, J. M. Bosqued, V. Perroomian, Z. Wang, D. Schriver, and R. L. Richard, The formation of the wall region: Consequences in the near earth magnetotail, *Geophys. Res. Lett.*, 19, 1739-1742, 1992b.
- Ashour-Abdalla, M., J. P. Berchem, J. Büchner, and L. M. Zelenyi, Shaping of the magnetotail from the mantle: Global and local structuring, *J. Geophys. Res.*, 98, 5651-5676, 1993.
- Baumjohann, W., G. Paschmann, and C. A. Cattell, Average plasma properties in the central plasma sheet, *J. Geophys. Res.*, 94, 6597-6606, 1989.
- Birmingham, T. J., Birkeland currents in an anisotropic, magnetostatic plasma, *J. Geophys. Res.*, 97, 3907-3917, 1992.
- Bosqued, J. M., M. Ashour-Abdalla, M. El Alaoui, L. M. Zelenyi, and A. Berthelier, Aureol-3 observations of new boundaries in the auroral ion precipitation, *Geophys. Res. Lett.*, 20, 1203-1206, 1993.
- Brittnacher, M. J. and E. C. Whipple, Chaotic jumps in the generalized first adiabatic invariant in current sheets, *Geophys. Res. Lett.*, 18, 1599-1602, 1991.
- Büchner, J., Correlation-modulated chaotic scattering in the Earth's magnetosphere, *Geophys. Res. Lett.*, 18, 1595-1598, 1991.
- Büchner, J., and L. M. Zelenyi, Deterministic chaos in the dynamics of charged particles near a magnetic field reversal, *Physics Letters A.*, 118, 395-399, 1986.
- Büchner, J., and L. M. Zelenyi, Regular and chaotic charged particle motion in magnetotaillike field reversals. 1. Basic theory of trapped motion, *J. Geophys. Res.*, 94, 11,821-11,842, 1989.

- Büchner, J., and L. M. Zelenyi, The separatrix tentacle effect of ion acceleration to the plasma sheet boundary, *Geophys. Res. Lett.*, *17*, 127-130, 1990.
- Büchner, J., and L. M. Zelenyi, Regular and chaotic charged particle motion in sheared magnetic field reversals. *Adv. Space Res.*, *11*, (9)177-(9)182, 1991.
- Burkhart, G. R. and J. Chen, Differential memory in the Earth's magnetotail, *J. Geophys. Res.*, *96*, 14,033-14,049, 1991.
- Burkhart, G. R., J. F. Drake, P. B. Dusenbery, and T. W. Speiser, A particle model for magnetotail neutral sheet equilibria, *J. Geophys. Res.*, *97*, 13,799-13,815, 1992.
- Chen, J., Nonlinear dynamics of charged particles in the magnetotail, *J. Geophys. Res.*, *97*, 15,011-15,050, 1992.
- Chen, J., and P. J. Palmadesso, Chaos and nonlinear dynamics of single-particle orbits in a magnetotail-like magnetic field, *J. Geophys. Res.*, *91*, 1499-1508, 1986.
- Cowley, S. W. H., A note on the motion of charged particles in one-dimensional magnetic current sheets, *Planet. Space Sci.*, *26*, 539-545, 1978.
- Cowley, S. W. H., and W. J. Hughes, *Planet. Space Sci.*, *31*, 73-90, 1983.
- Dusenbery, P. B., G. R. Burkhart, T. W. Speiser, and F. Hall, The effect of a nonzero B_y on particle motion in the tail, *Eos Trans. AGU*, *74*, 520, 1993 (abstract).
- Fairfield, D. H., On the average configuration of the geomagnetic tail, *J. Geophys. Res.*, *84*, 1950-1958, 1979.
- Harris, E. G., On a plasma sheath separating regions of oppositely directed magnetic field, *II Nuovo Cimento*, *23*, 115-121, 1962.
- Heinemann, M., and D. H. Pontius, Jr., Representations of currents and magnetic fields in anisotropic magnetohydrostatic plasma, 2, General theory and examples, *J. Geophys. Res.*, *96*, 17,609-17,626, 1991.

- Iijima, T., and T. A. Potemra, Large-scale characteristics of field-aligned currents associated with substorms, *J. Geophys. Res.*, *83*, 599-615, 1978.
- Karimabadi, H., P. L. Pritchett, and F. V. Coroniti, Particle orbits in two-dimensional equilibrium models for the magnetotail, *J. Geophys. Res.*, *95*, 17,153-17,166, 1990.
- Kaufmann, R. L., and P. M. Kintner, Upgoing ion beams, 2, Fluid analysis and magnetosphere-ionosphere coupling, *J. Geophys. Res.*, *89*, 2195-2210, 1984.
- Kaufmann, R. L., D. J. Larson, P. Beidl, and C. Lu, Mapping and energization in the magnetotail, 1, Magnetospheric boundaries, *J. Geophys. Res.*, *98*, 9307-9320, 1993a.
- Kaufmann, R. L., D. J. Larson, and C. Lu, Mapping and energization in the magnetotail, 2, Particle acceleration, *J. Geophys. Res.*, *98*, 9321-9333, 1993b.
- Kaufmann, R. L., and C. Lu, Magnetotail current carriers: Quasiadiabatic orbits, *J. Geophys. Res.*, *98*, 15,447-15,465, 1993c.
- Kaymaz, Z., G. L. Siscoe, J. G. Luhmann, R. P. Lepping, and C. T. Russell, IMF control of geotail magnetic field geometry: IMP-8 observations, submitted to *J. Geophys. Res.*, 1994.
- Lui, A. T. Y., Characteristics of the cross-tail current in the Earth's magnetotail, in *Magnetospheric Currents*, T. A. Potemra, editor, pp. 158-170, American Geophysical Union, Washington, DC, 1984.
- Pontius, D. H., Jr., On Vasyliunas's equivalent conductivity formalism, *J. Geophys. Res.*, *97*, 19,527-19,529, 1992.
- Pulkkinen, T. I., D. N. Baker, R. J. Pellinen, J. Büchner, H. E. J. Koskinen, R. E. Lopez, R. L. Dyson, and L. A. Frank, Particle scattering and current sheet stability in the geomagnetic tail during the substorm growth phase, *J. Geophys. Res.*, *97*, 19,283-19,297, 1992.
- Savenkov, B. V., L. M. Zelenyi, M. Ashour-Abdalla, and J. Büchner, Regular and chaotic aspects of charged particle motion in a magnetotail-like field with a neutral line, *Geophys. Res. Lett.*, *18*, 1587-1590, 1991.

- Sergeev, V. A., Penetration of the B_y -component of the interplanetary magnetic field (IMF) into the tail of the magnetosphere, *Geomag. and Aeronomy*, 27, 528-531, 1987.
- Sibeck, D. G., G. L. Siscoe, J. A. Slavin, E. J. Smith, B. T. Tsurutani, and S. J. Bame, Magnetic field properties of the distant magnetotail magnetopause and boundary layer, *J. Geophys. Res.*, 90, 9561-9575, 1985.
- Siscoe, G., and N. Maynard, Distributed two-dimensional region 1 and region 2 currents: Model results and data comparison, *J. Geophys. Res.*, 96, 21,071-21,085, 1991.
- Sonnerup, B. U. Ö., Adiabatic particle orbits in a magnetic null sheet, *J. Geophys. Res.*, 76, 8211-8222, 1971.
- Speiser, T. W., Conductivity without collisions or noise, *Planet. Space Sci.*, 18, 613-622, 1970.
- Tsyganenko, N. A., A magnetospheric magnetic field model with a warped tail current sheet, *Planet. Space Sci.*, 37, 5-20, 1989.
- Vasyliunas, V. M., The interrelationship of magnetospheric processes, *Earth's Magnetospheric Processes*, B. M. McCormac, ed., D. Reidel Publishing Co., Dordrecht, Holland, 29-38, 1972.
- Wolf, R. A. and D. H. Pontius, Jr., Particle drift in the earth's plasma sheet, *Geophys. Res. Lett.*, 20, 1455-1458, 1993.

Figure Captions

Fig. 1. Particle orbits that follow invariant tori (a) ring-like torus, (b) half of a split torus, (c) full split torus.

Fig. 2. Dependence upon κ of the normalized cross-tail drift velocity distribution $\langle v_y(z) \rangle / v_o$ when $B_{y0} = 0$.

Fig. 3. Sketches of B_y produced by different sources.

Fig. 4. (a) Root mean square pitch angle changes for protons resulting from current sheet interactions near the $N = 1$ resonance (b) Fraction of the protons that left the current sheet on the same side from which they entered.

Fig. 5. Sample proton orbits in fields with different B_{y0} .

Fig. 6. Peak value of the normalized cross-tail drift velocity near the $N = 1$ resonance.

Fig. 7. Normalized distribution of the cross-tail drift velocity for several B_{y0} . The ion energy corresponds to the $N = 1$ resonance.

Fig 8. Root mean square pitch angle changes for protons resulting from current sheet interactions near the $N = 2$ resonance.

Fig. 9. Sample proton orbits in model fields with $B_{y0} = \pm 2$ nT.

Fig. 10. (a) Root mean square pitch angle changes for protons resulting from current sheet interactions near the $N = 2$ ($W = 900$ eV) and $N = 3$ ($W = 3.6$ keV) resonances. (b) peak value of the normalized cross-tail drift velocity.

Fig. 11. Root mean square pitch angle changes for protons resulting from current sheet interactions near the $N = 6$ ($W = 1.8$ keV) and $N = 7$ ($W = 3.4$ keV) resonances.

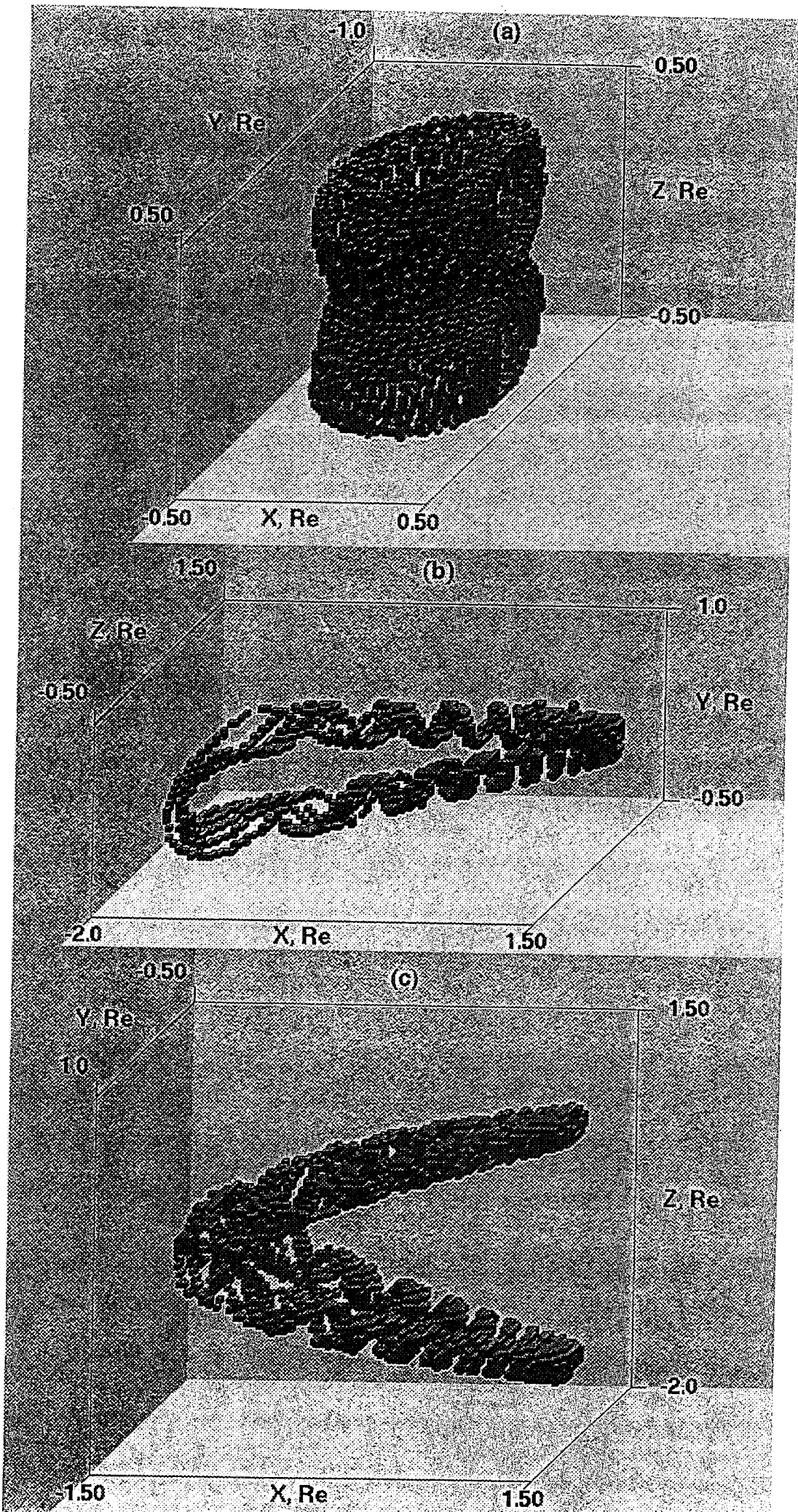
Fig. 12. Pitch angles for individual protons before (α_i) and after (α_f) a current sheet interaction.

Fig. 13. Root mean square pitch angle changes for protons resulting from current sheet interactions near the $N = 2$ resonance.

Fig. 14. Sketches of contours of constant κ , the ion and electron cross-tail drift velocities V_{di} and V_{de} , and the number of ions and electrons in a unit flux tube N .

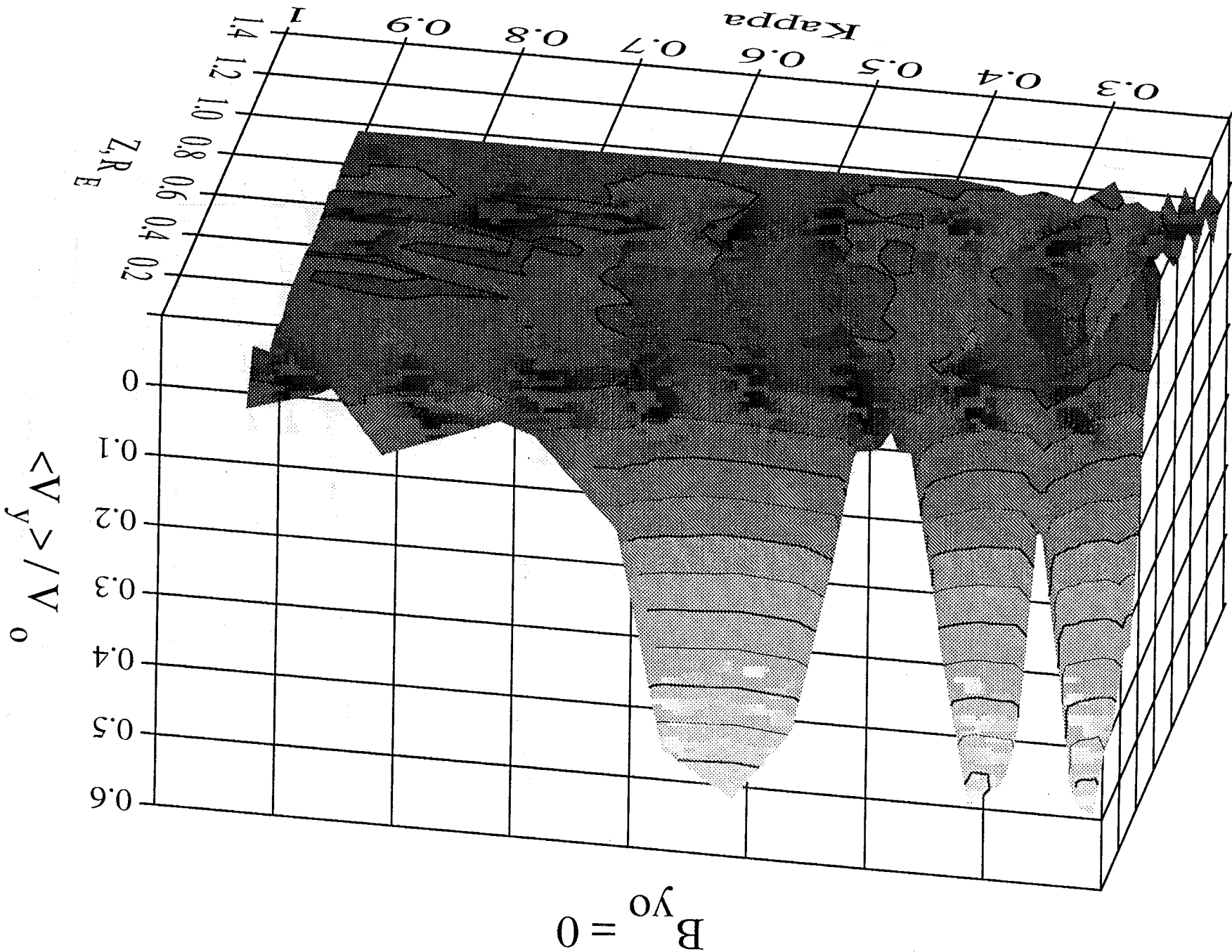
Fig. 15. Average cross-tail drift velocities V_{di} and V_{de} , flux tube content N , and fluxes of ions and electrons for simple models of the transition region between stochastic and resonant orbits, as shown in Figure 14a.

Fig. 16. (a) x, y locations of $z = 0$ plane crossings for a group of ions in the three-dimensional T89 Kp = 4 model (b) The κ parameter evaluated at each $z = 0$ plane crossing.

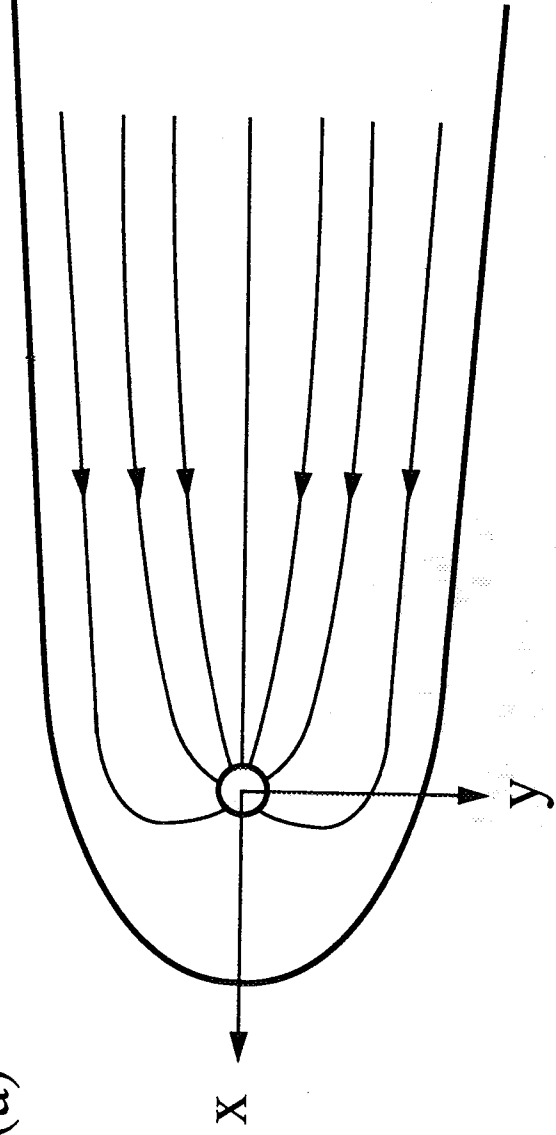


Figs 1

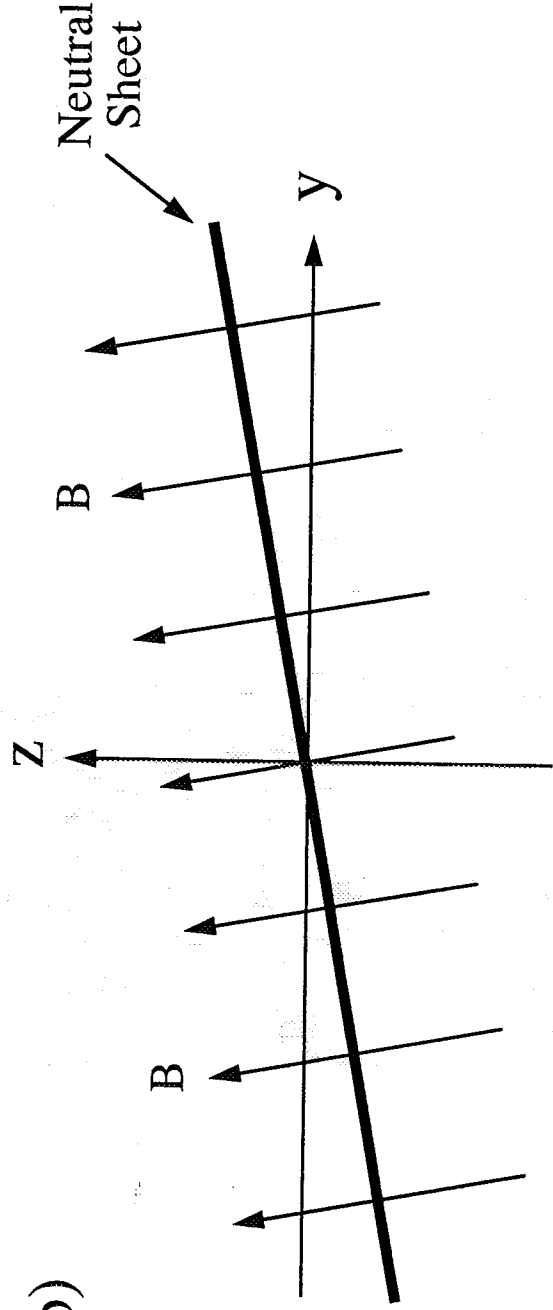
Figure 2



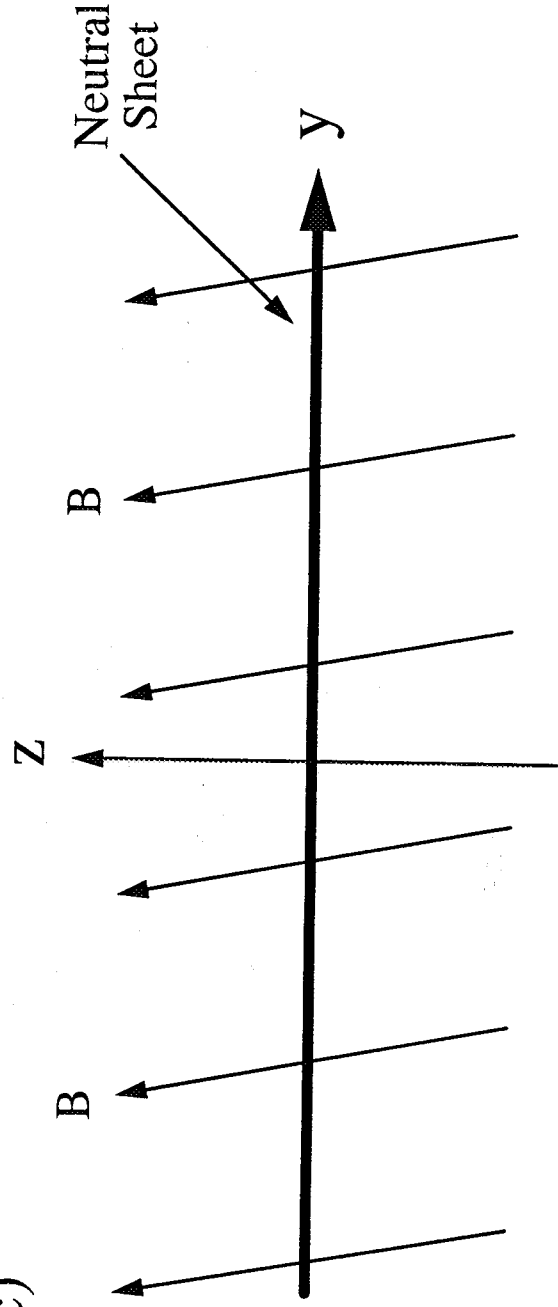
(a)



(b)



(c)



$\langle \Delta\alpha \rangle$, degrees

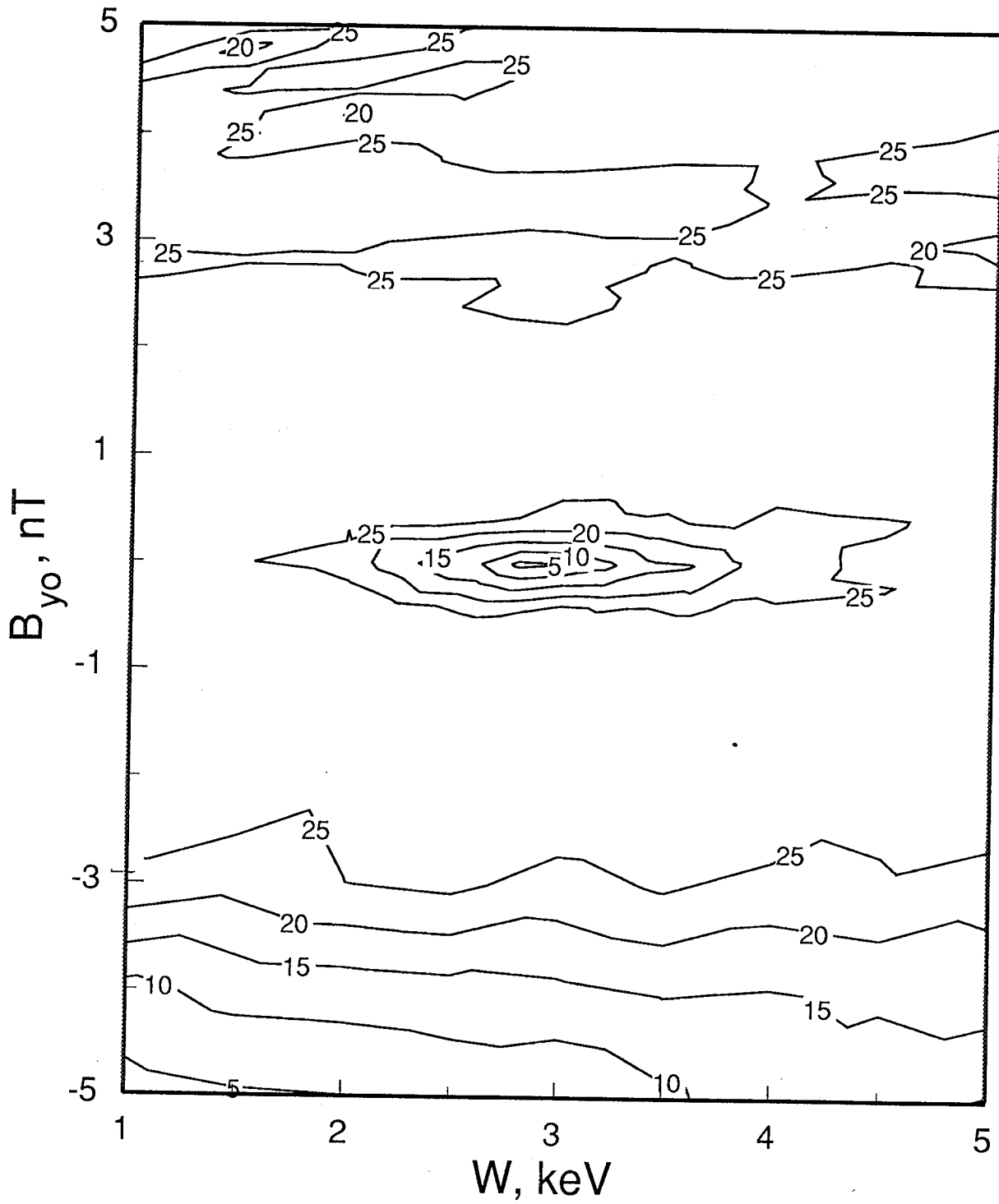


Figure 4a

Fraction Reflected

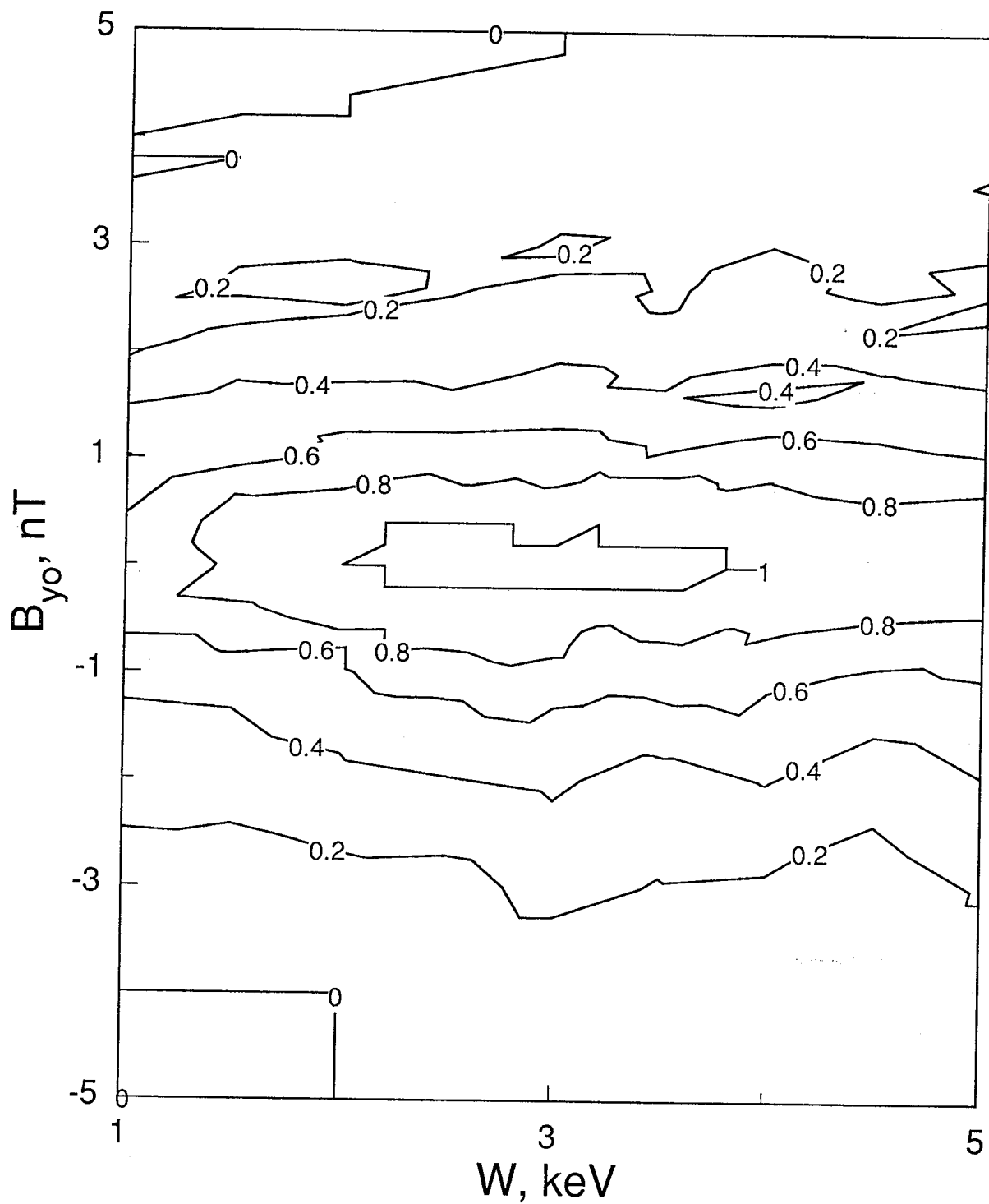


Figure 4b

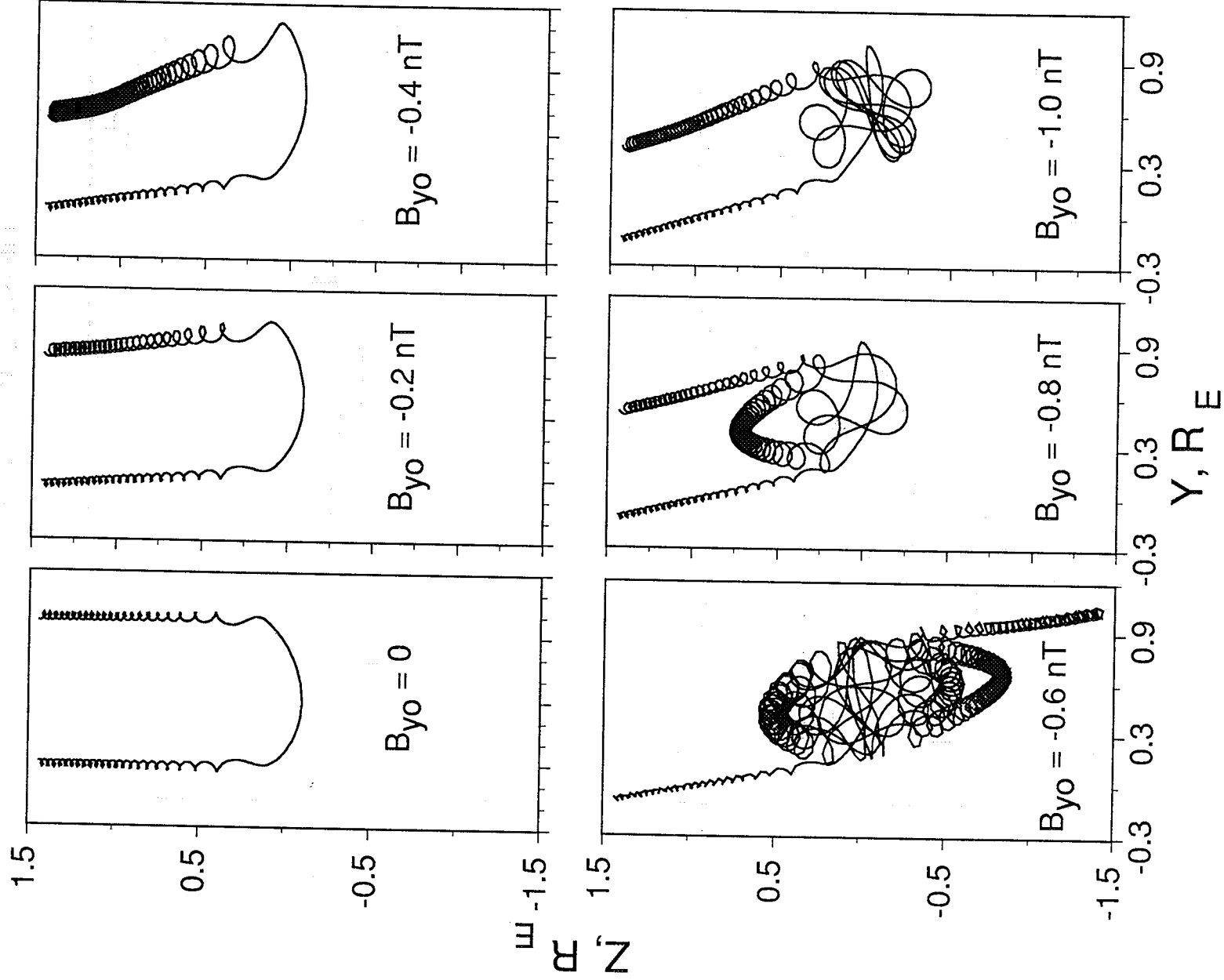


Figure 5

peak $\langle V_y \rangle / V_0$

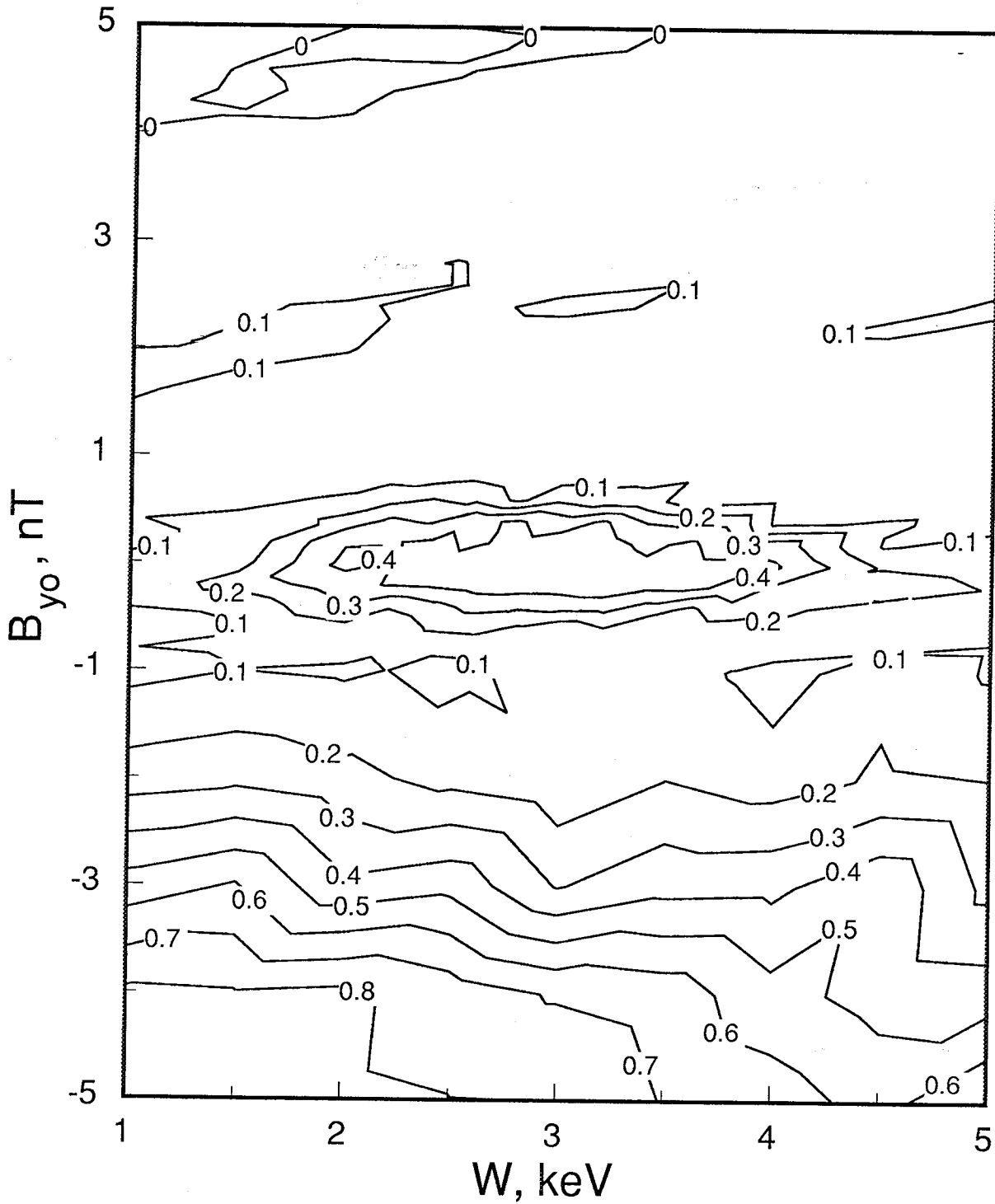


Figure 6

Figure 7

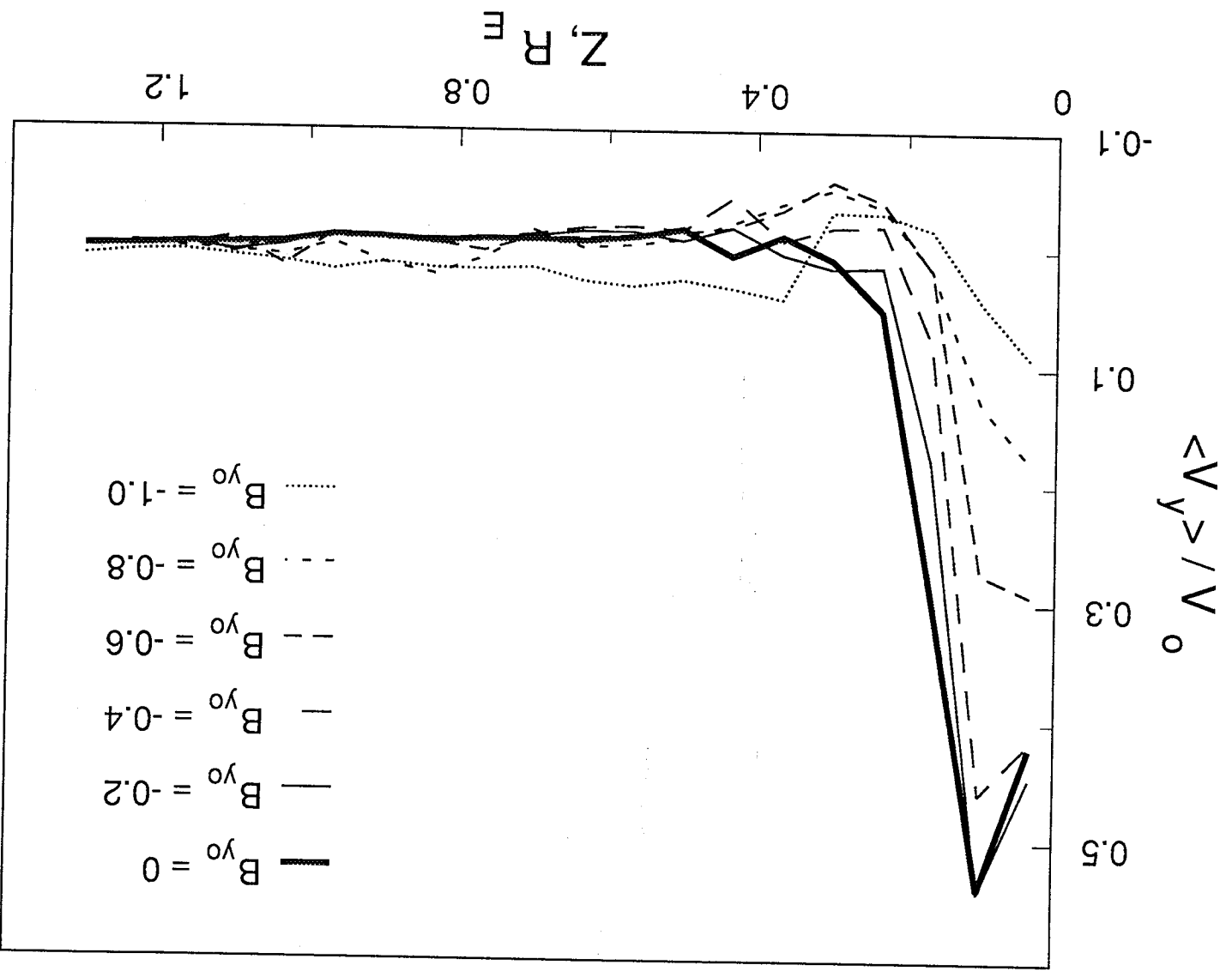


Figure 8

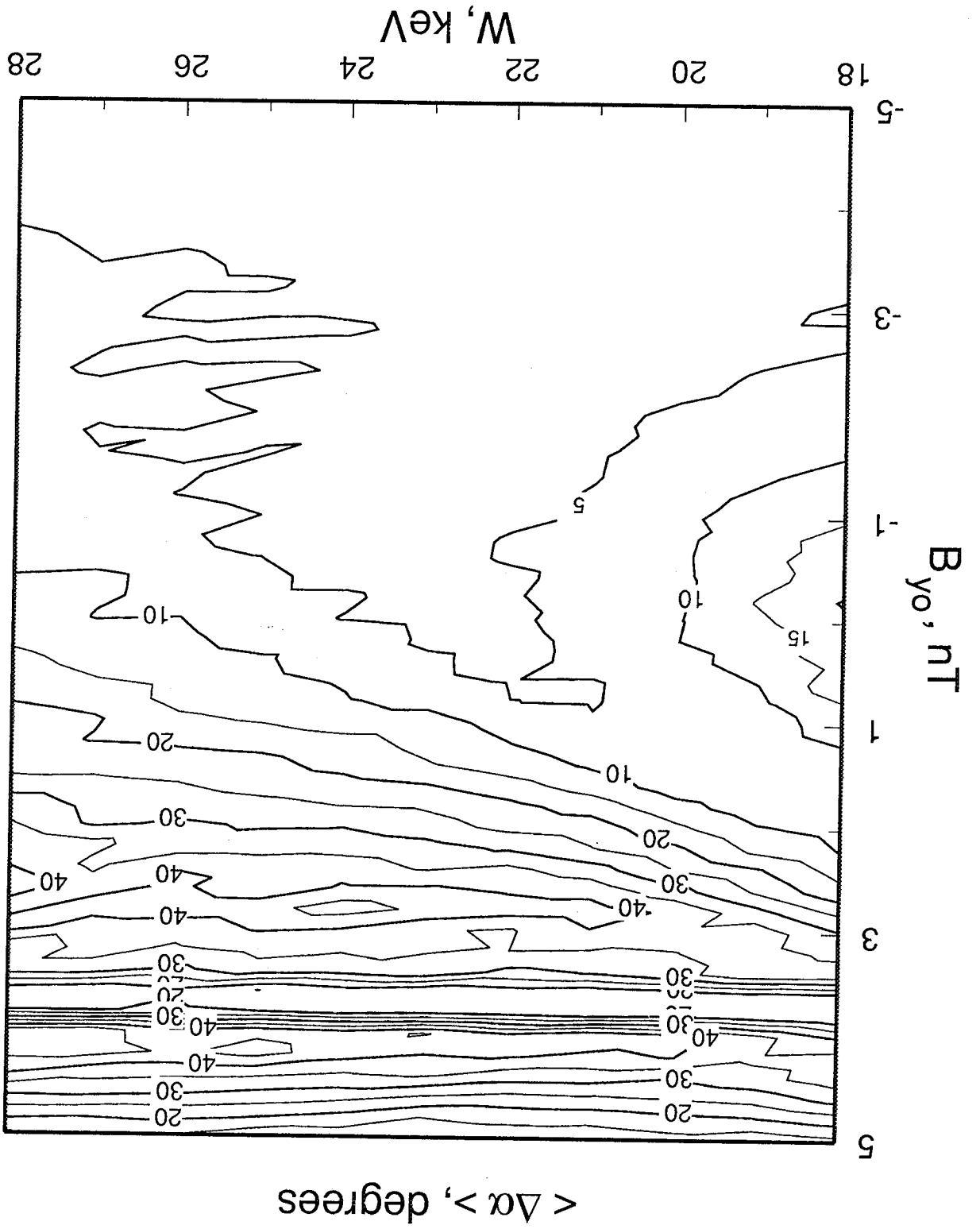
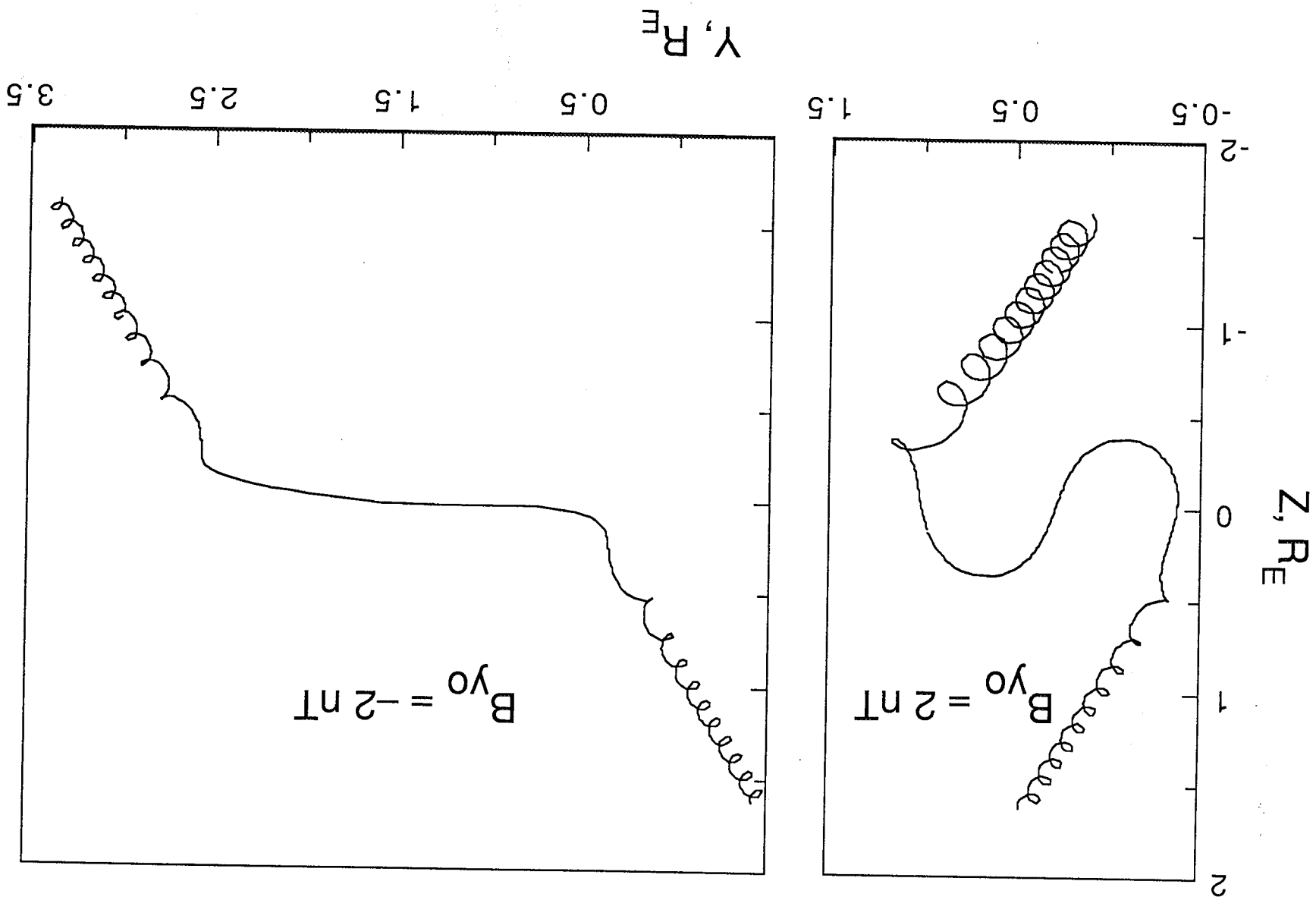


Figure 9



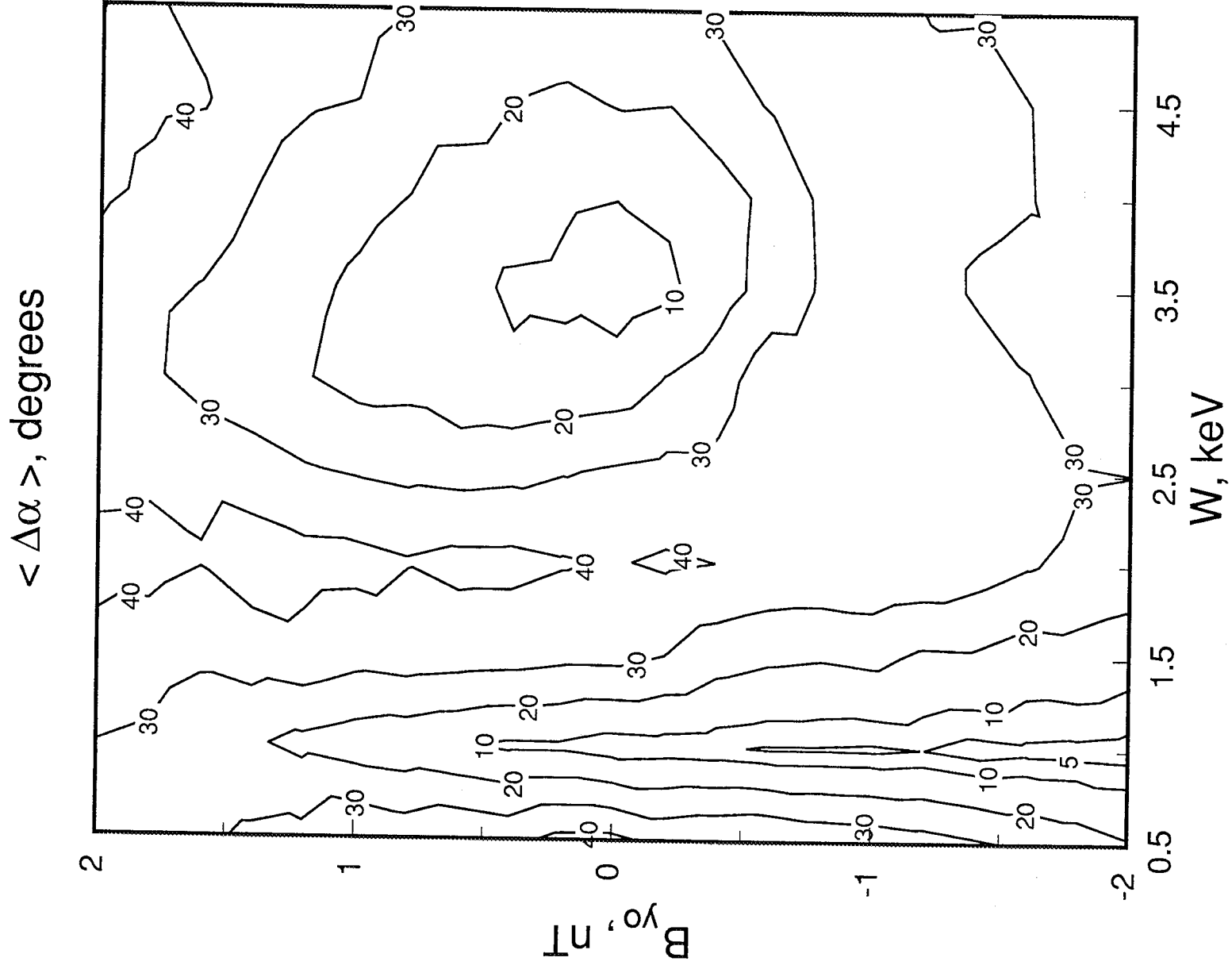


Figure 10a

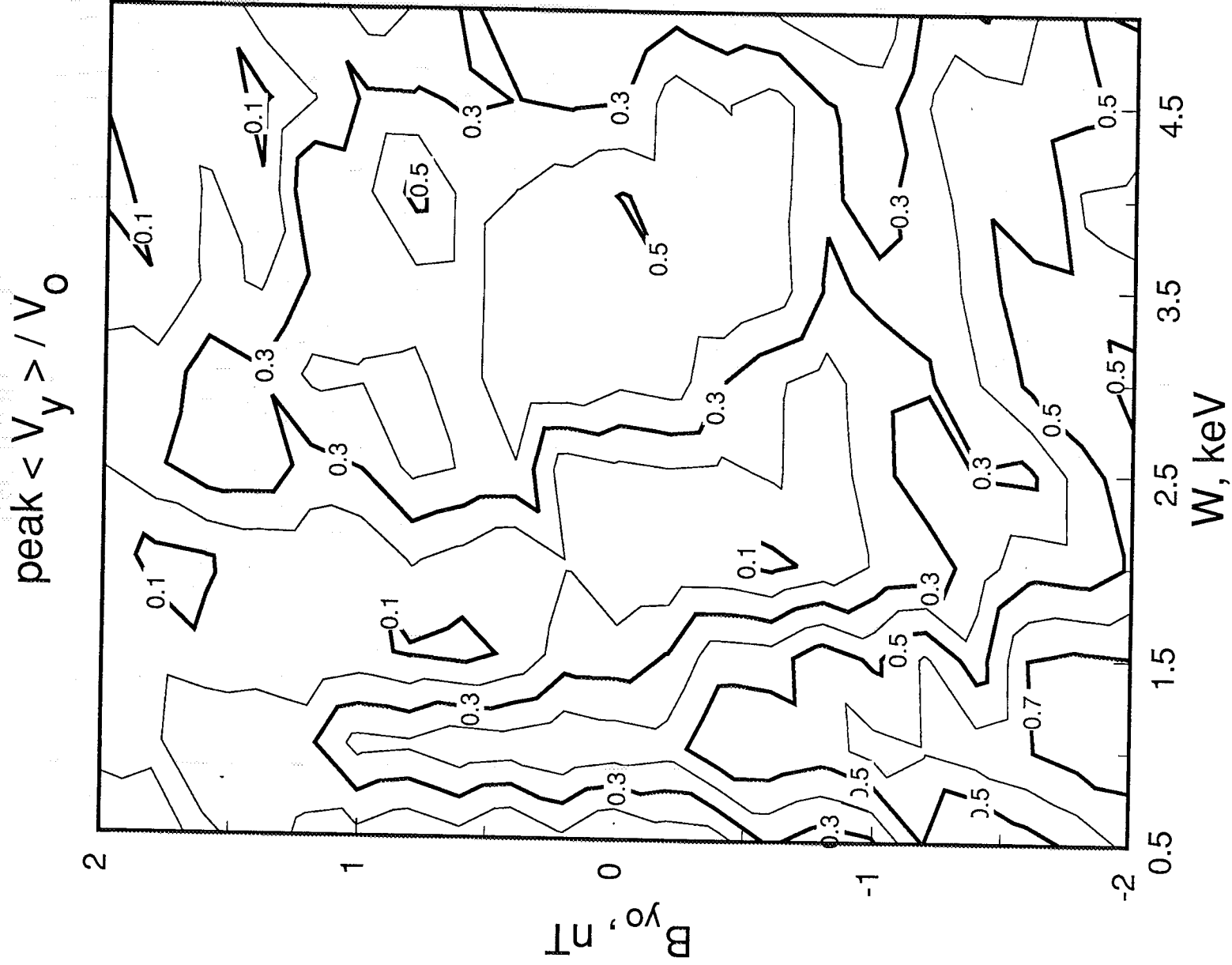


Figure 10b

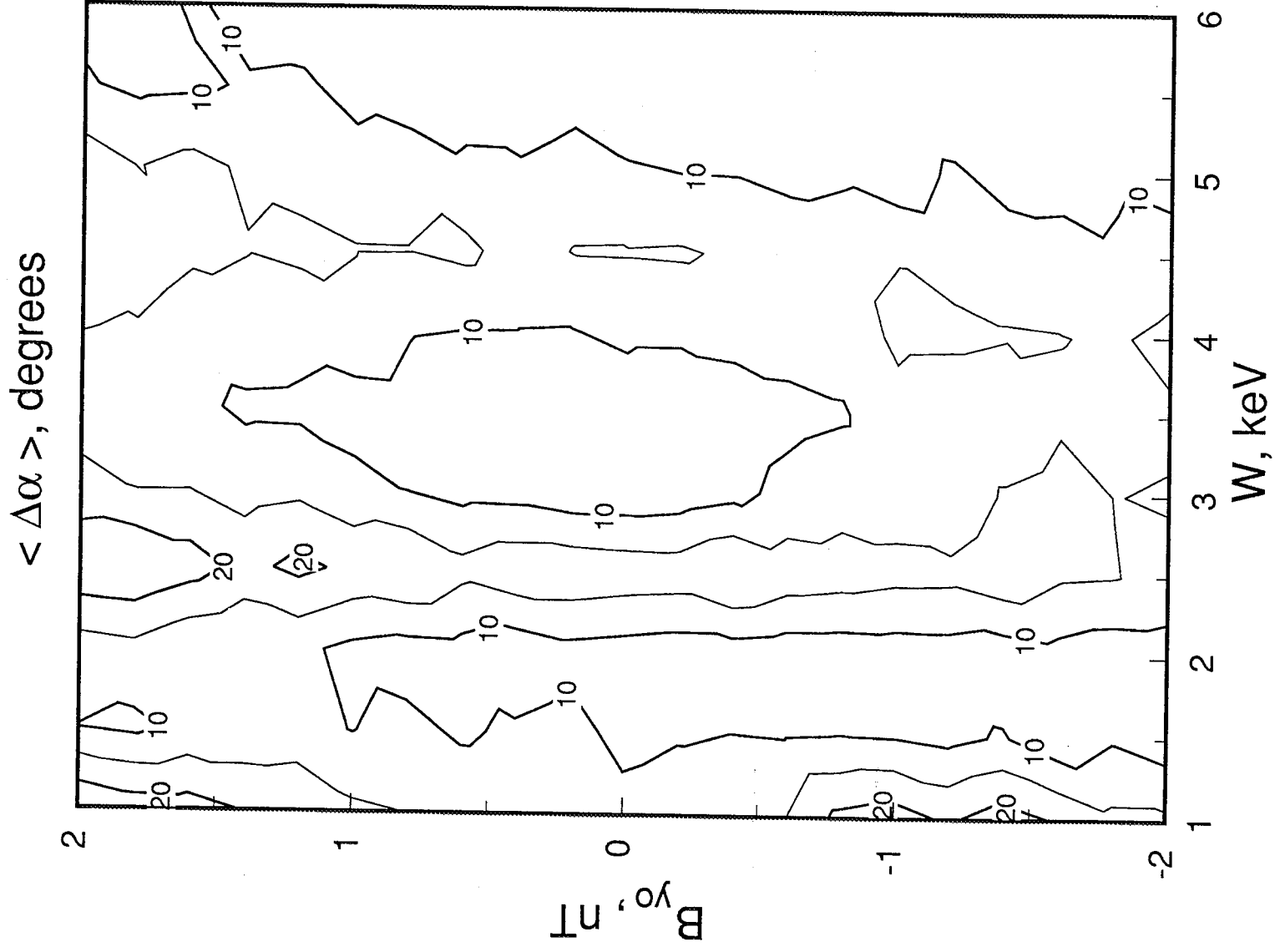
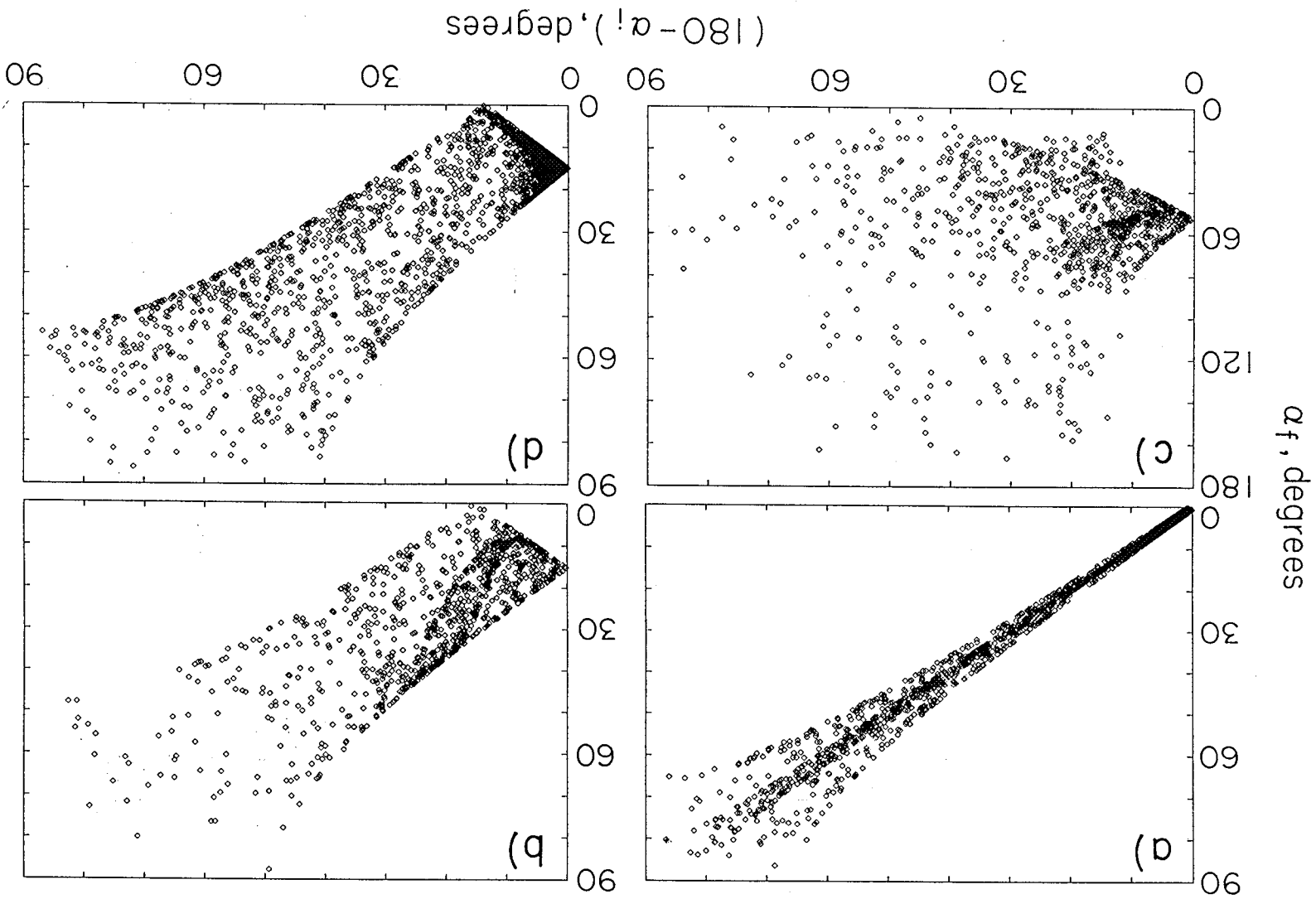


Figure 12



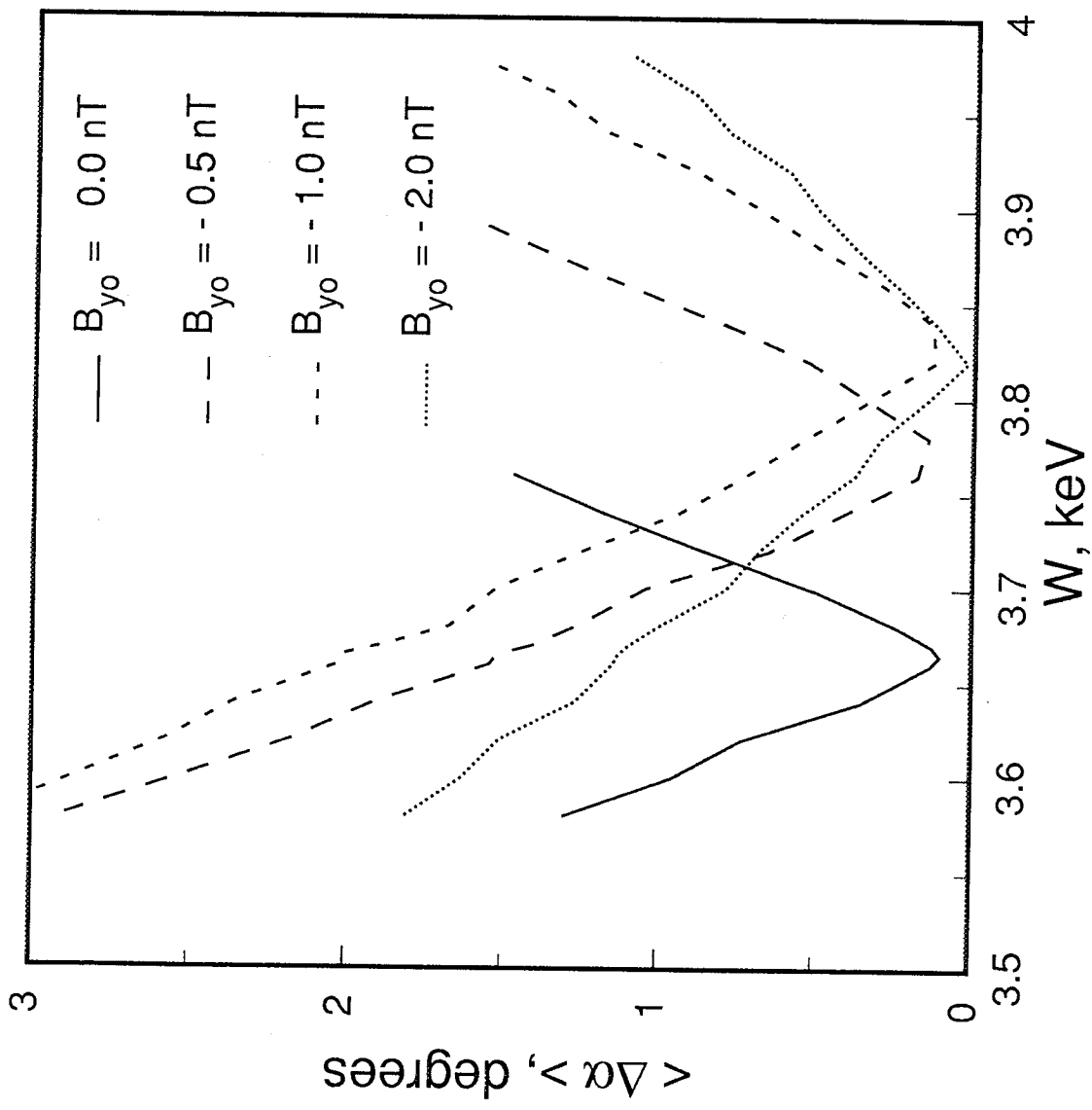


Figure 13

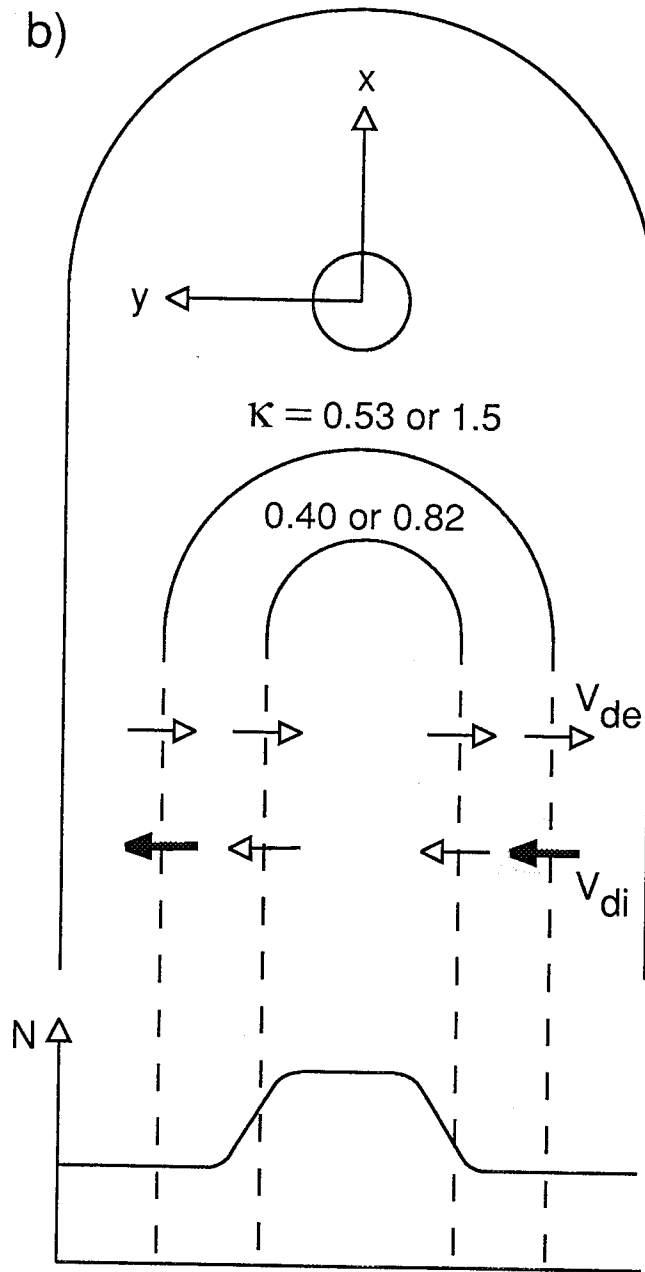
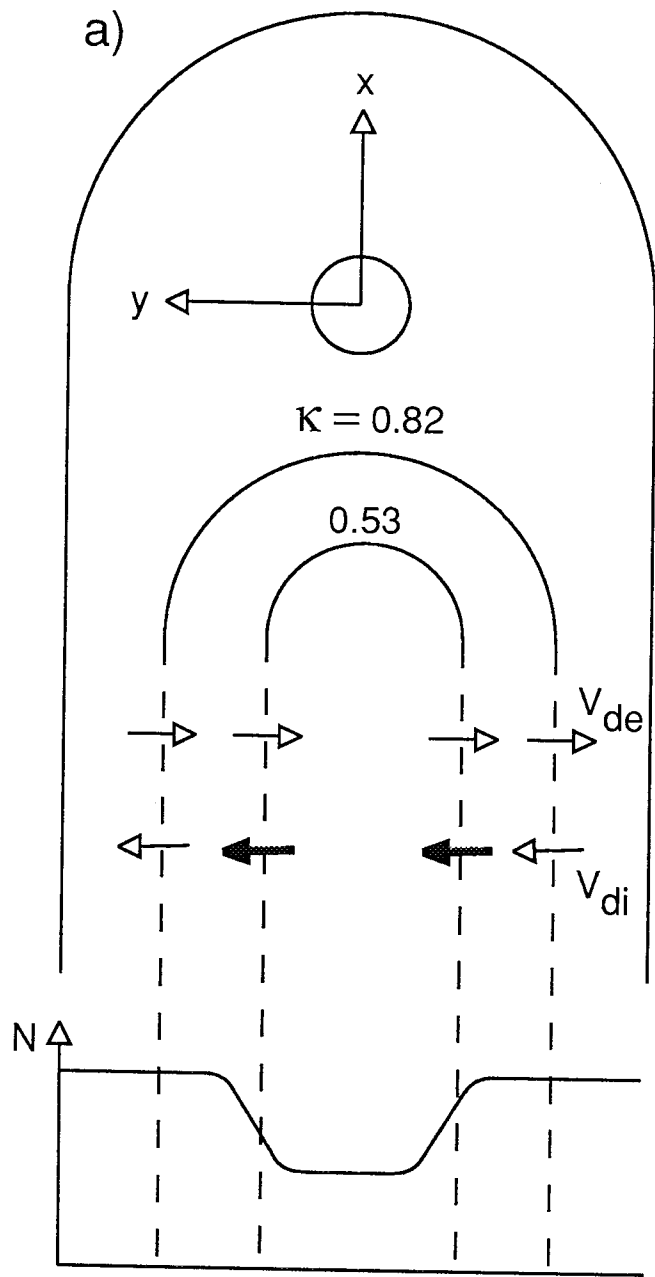
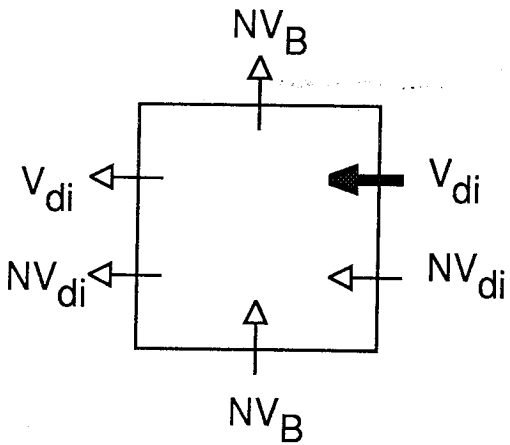


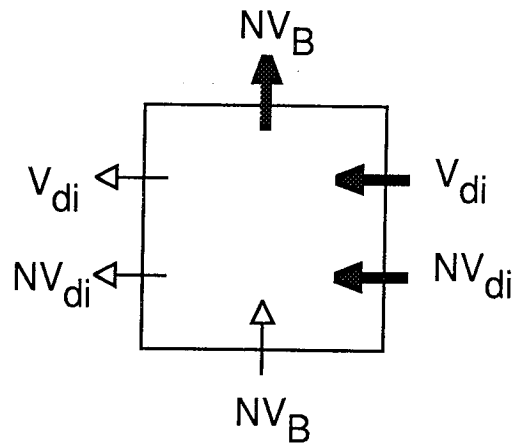
Figure 14

dusk side

a)

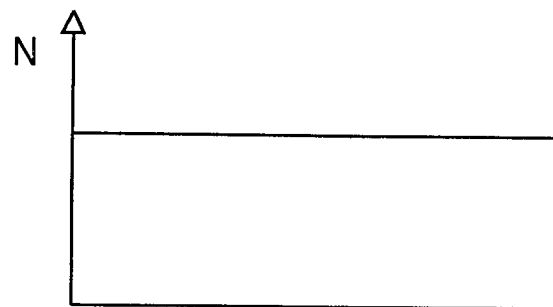
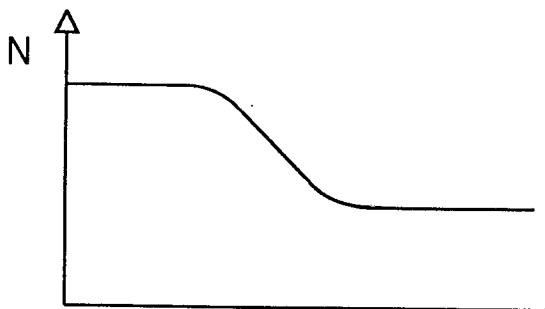
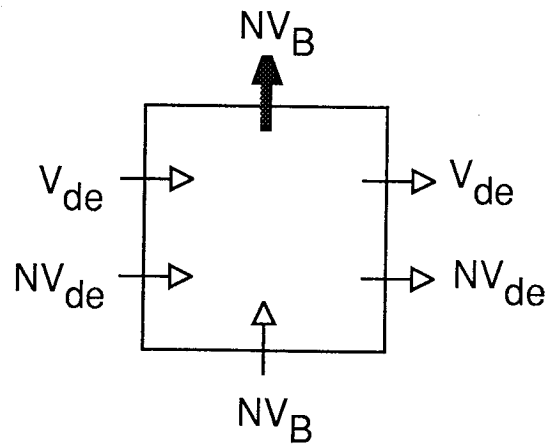
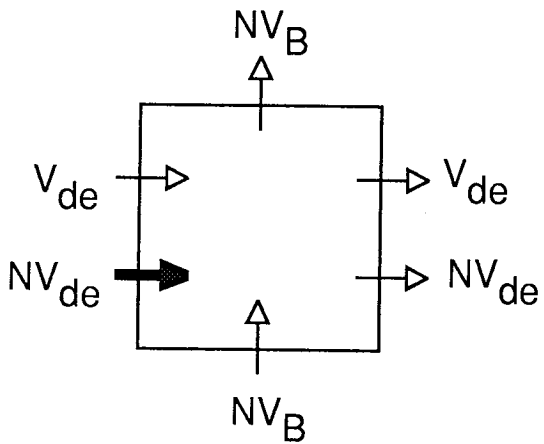


b)



ions

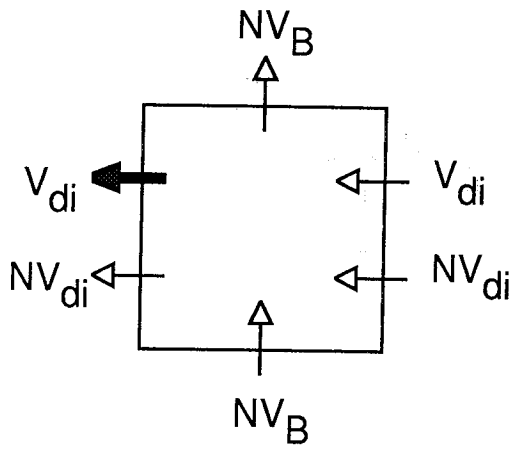
electrons



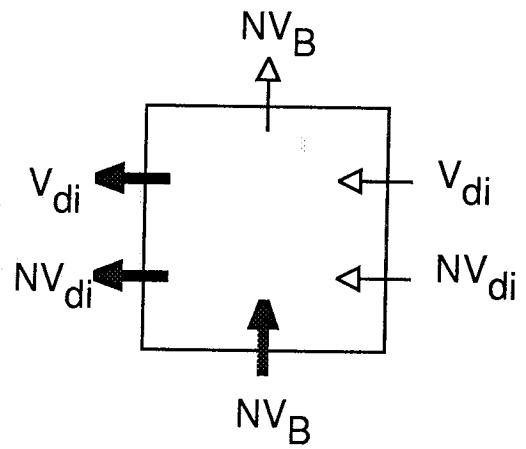
2008

dawn side

c)



d)



ions

electrons

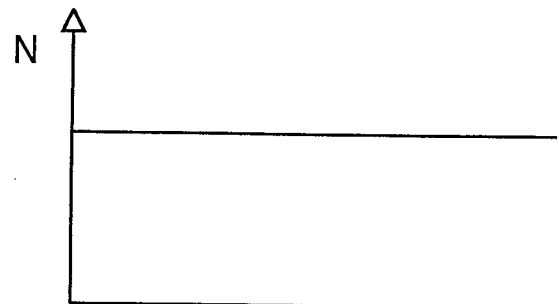
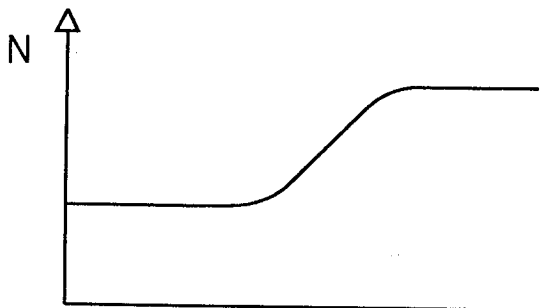
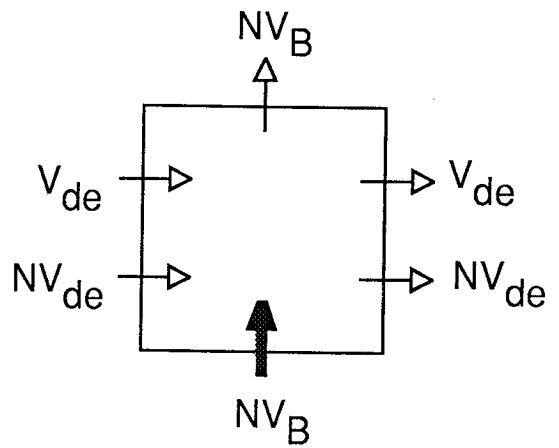
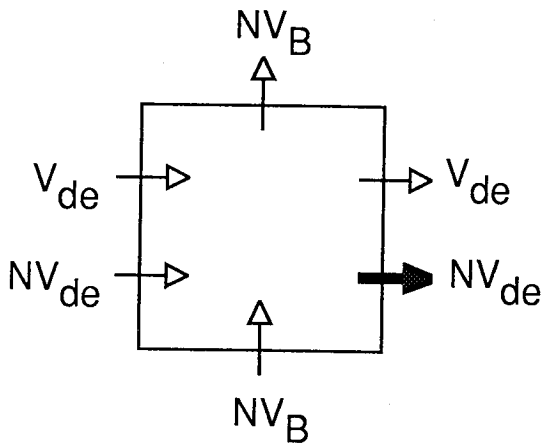


Figure 15 c, d

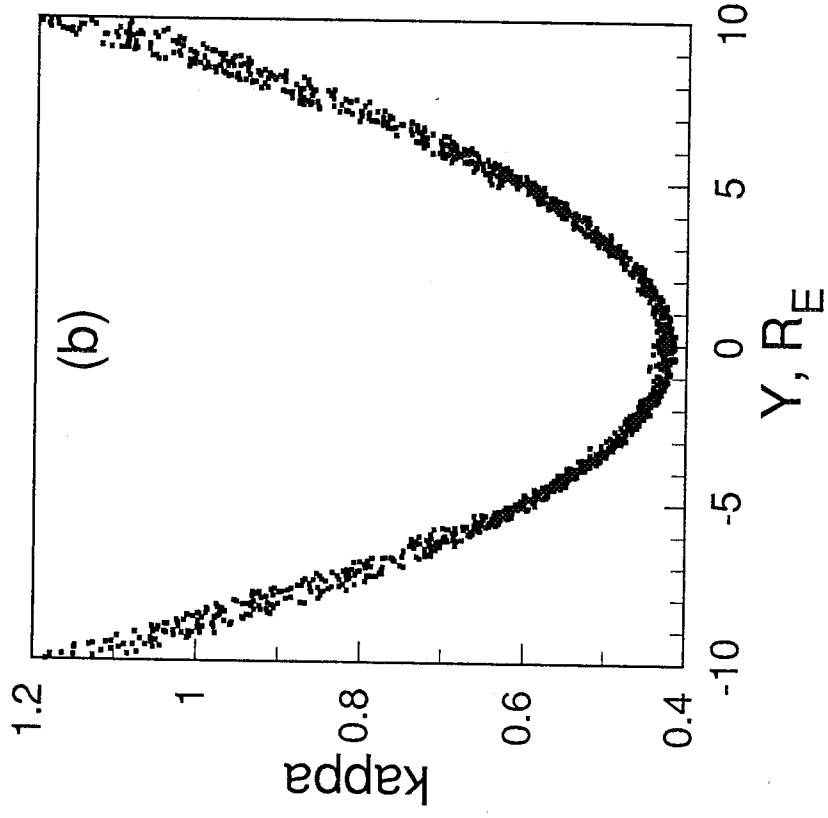
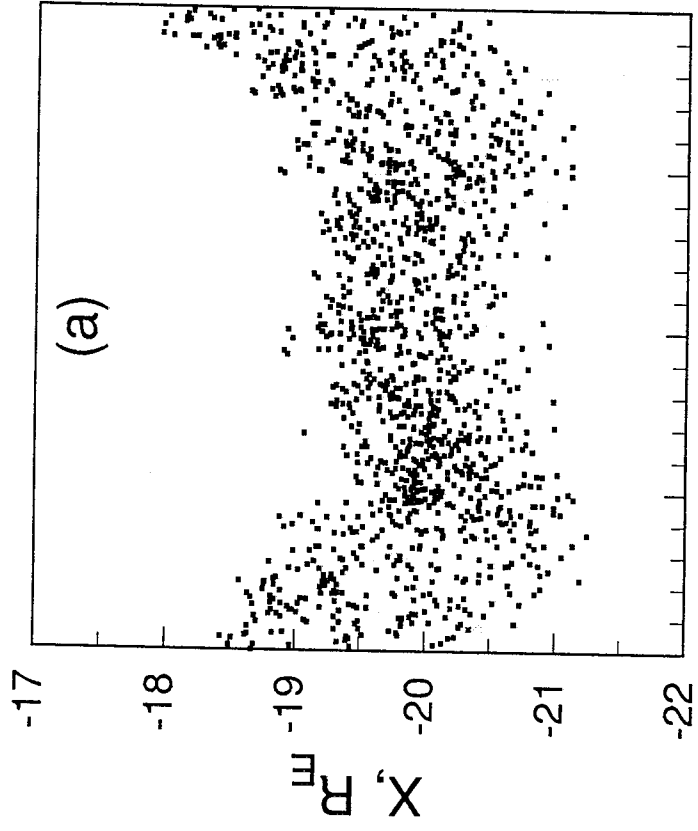


Figure 16